Strontium Monoxide Measurements in Methane-air Flames

A Thesis Presented for the
Master of Science
Degree
The University of Tennessee, Knoxville

Bobby J. Wimberly
December 2015

Copyright © 2015 by Bobby J. Wimberly

All rights reserved.

ACKNOWLEDGEMENTS

I would like to thank my thesis advisor, Dr. Christian Parigger and my committee members, Dr. Lloyd Davis and Dr. Horace Crater for their support and guidance throughout my time at UTSI. In addition, I would like to thank Dr. Robert A. Reed for his advice and assistance during the preparation of this thesis.

ABSTRACT

The spectroscopy of alkaline earth metal compounds has been an area of active research for several decades. This is at least in part stimulated by the application of these compounds to practical areas ranging from technology to medicine. The use of these compounds in the field of pyrotechnics was the motivation for a series of flame emission spectroscopy (FES) experiments with strontium containing compounds. Specifically, strontium monoxide (SrO) is studied as a candidate radiator for the diagnostic of methane-air flames.

SrO emissions have been observed in flames with temperatures in the range of 1200-1600-K for two compounds: strontium hydroxide and strontium chloride. Comparisons are made of the measured SrO spectra to simulated spectra in the near-infrared region (700-900-nm) and conditions of local thermodynamic equilibrium (LTE) are discussed.

TABLE OF CONTENTS

1 Introduction 1

1.1 Spectroscopic Techniques 1
1.2 Experimental Data 2
1.3 Diagnostic Techniques 3
1.4 Spectra of Diatomic Molecules 4

2 Experiment 8

2.1 Burner Apparatus 8
2.2 Spectrometer 9
2.3 Simulation 11

3 Results and Discussion 16

3.1 Survey of Measured Spectra 16
3.2 SrO Formation and Emissions 17
3.3 Simulated Spectra 20
3.4 Flame Diagnostics 28

3.4.1 SrO A-X Bands 29

3.4.2 C_2 Swan Band 32

4 Conclusions and Recommendations 36

References 38

Appendices 43

Vita 62

LIST OF TABLES

Table 2-1: Experiment Summary 10

Table 2-2: Spectrometer Wavelength Calibration 11

Table 2-3: Spectroscopic constants for $^{88}Sr^{16}O$ 14

Table 2-4: Spectroscopic constants for C_2 14

Table 3-1: Example CEA results for $SrCl_2$-doped flame at 1613-K 18

Table 3-2: Dissociation energies of strontium molecular bonds 19

LIST OF FIGURES

Figure 2-1: Burner apparatus. 10

Figure 3-1: Survey of species in experimental spectra. 18

Figure 3-2: SrO-isolated spectrum. 21

Figure 3-3: Simulated relative line strengths of the SrO $A^1\Sigma^+$-$X^1\Sigma^+$ band system. 22

Figure 3-4: Spectrometer resolution determined from Sr I atomic line. 24

Figure 3-5: SrO A-X system: Simulated versus recorded spectra. 25

Figure 3-6: Effect of additional state transitions on simulated spectra. 27

Figure 3-7: SrO A-X system in experiments 7-10, normalized to the $\Delta v = 1$ band head signals. 30

Figure 3-8: Temperature trends in the measured SrO $\Delta v = 3$ band. 31

Figure 3-9: Effect of temperature on the band head shape. 33

Figure 3-10: C_2 d-a $\Delta v = 0$: Simulated versus recorded spectra. 34

Figure D-1: NMT fit window for experiment 2. 58

Figure D-2: NMT fitted spectrum versus recorded spectrum for experiment 2 59

Figure D-3: NMT fit window for experiment 8. 60

Figure D-4: NMT fitted spectrum versus recorded spectrum for experiment 8 61

1 INTRODUCTION

Alkaline earth metals have been studied for a wide variety of applications. These range from technological and industrial applications such as diluted magnetic semiconductors (DMSs) [1] and environmentally safe catalysis of chemical reactions [2] to biomechanical applications such as bioresorbable materials and tissue engineering [3]. One of the more common applications of alkaline earth metal compounds, however, is their use in pyrotechnics as flame colorants [4]. In particular, strontium compounds have long been used to enhance the color of flames in the red visible region (600-700-nm).

For these and other reasons, the spectroscopy of strontium compounds has been an ongoing area of active study [5-10]. The goal of this work has been to investigate the application of strontium monoxide (SrO) emissions in the near-infrared (NIR) spectral region to the diagnostics of hydrocarbon-air flames. Experiments performed in 2011 provide both the data and the impetus for the current investigation as described in the sections to follow.

1.1 Spectroscopic Techniques

Numerous spectroscopic techniques have been employed in the investigation of strontium based molecular emissions. Among these are techniques that rely on laser stimulation to provide excitation, in particular, laser ablation molecular isotopic spectrometry (LAMIS) [11], a technique closely related to laser induced breakdown spectroscopy (LIBS) [12], and optical-optical double-resonance (OODR) [13] spectroscopy. Other, earlier studies used techniques involving induced fluorescence from high power incandescent sources [8].

Flame emission spectroscopy (FES), however, is one of the earliest tools [14] for the study of atomic and molecular emissions. In FES, a flame is used as the excitation

energy source to produce spectral emissions from atomic and molecular species. Numerous methods exist to introduce the species under study into the flame. These range from inserting a wire or filament of the test material into the flame to injecting the material in the gaseous form. One of the simplest methods is to dissolve the compound under study and nebulize the solution for injection into the flame. In this method, the flame acts first to desolvate and decompose the compound under study into atomic and molecular species, and subsequently provides the excitation energy to produce the desired emissions.

1.2 Experimental Data

In 2011, FES experiments were performed to provide data to guide the development of high temperature band models for selected strontium molecular transitions known to contribute to the visible emissions in pyrotechnic flames. Specifically, strontium monohydroxide (SrOH) and strontium monochloride (SrCl) transitions were investigated. Both molecules have been identified as red (600-700-nm) emitters in the study of pyrotechnics [4].

The goal of the experiments was to vary the flame temperature for fixed amounts of colorant compound and measure the visible spectral output. Spectral data would then be used to guide the determination of spectroscopic constants, which at the time were either unavailable or highly uncertain for the specific bands of interest. Control of the flame temperature was to be achieved by the adjustment of the fuel/air equivalence ratio by varying the flow of air while holding the fuel flow constant.

It was found, however, that failure to operate the nitrogen curtain of the burner system to isolate the methane-air flame from the atmosphere caused the flame to become “self-regulating” [15]. As a result, the actual equivalence ratio achieved was unknown. A natural outcome of the experimentally undetermined equivalence ratio is the loss of temperature control, a key parameter for the experiment. While temperature was

monitored by a thermocouple inserted into the flame, the question was raised as to the possible utility of spectral emissions of available constituents as non-intrusive flame diagnostics.

1.3 Diagnostic Techniques

While a procedure has been proposed to determine hydrocarbon-air flame equivalence ratio non-intrusively [16], it depends on the ratio of OH to CH emissions. However, the OH feature used for this procedure occurs in an ultraviolet region outside of the measured spectral range. More importantly, equivalence ratio is only one factor that controls the flame temperature, which is the key parameter of interest for the current investigations. Several methods do exist however for deriving flame temperature directly from spectral radiant intensities.

One well-established approach involves fitting a blackbody (Planck) distribution to the incandescent emissions in the measured spectra. Unfortunately, the occurrence of rich distributions of molecular bands and large overlap of spectral features in the data make this approach ineffective for this study.

The Boltzmann plot method [17, 18] is another well-established technique wherein temperature is determined from atomic line distributions such as the hydrogen Balmer Series [19] or molecular rotation-vibration band ratios. However, the data available from experiment are not well resolved, making the atomic line and molecular band ratios complex to compute. Modified Boltzmann plot techniques have been used to overcome the problems associated with poor resolution and band overlap [20], however these were not pursued due to the complexity of the observed spectra.

Finally, computer simulations can be used to fit experimental spectra with temperature as a fit parameter [21, 22]. For the current study, it is this approach that has been investigated. While several software packages are available that model the spectra of

simple molecules, the one used for this study is PGOPHER [23], a program developed at the University of Bristol for simulating rotational, vibrational and electronic structure.

The rotation-vibration-electronic (rovibronic) $A^1\Sigma^+ - X^1\Sigma^+$ transition bands of strontium monoxide (SrO) were identified in the measured spectra and have been analyzed for utility in the characterization of the experimental flame temperature. SrO band features for several vibronic transitions are observable in the experimental data making it a good candidate for flame diagnostic analysis. At the same time, the spectra of diatomic molecules have been well studied [17, 24-26] and present the simplest case for simulation making the SrO based analysis more straightforward as compared to that of other more complex molecules found in the flame.

1.4 Spectra of Diatomic Molecules

SrO is a heteronuclear diatomic molecule and therefore a brief review of the quantum mechanical treatment of diatomic spectra seems in order. Of particular interest to the current investigation are the details of the calculation of rovibronic line strengths. The brief derivation herein follows that of Thorne [18].

For a diatomic molecule the *electric dipole operator* $\boldsymbol{\mu}$ is

$$\boldsymbol{\mu} = \sum_i q_i \boldsymbol{r}_i + \sum_j q_j \boldsymbol{R}_j, \tag{1}$$

where $\boldsymbol{r}_i$ are the electronic coordinates and $\boldsymbol{R}_j$ the nuclear coordinates.

The line strength for a given rovibronic transition is given by

$$S = \sum_{m',m''} \left| \int \psi'^{*} \boldsymbol{\mu}\, \psi'' d\boldsymbol{r} \right|^2, \tag{2}$$

Here, ψ'' and ψ' are the total wavefunctions for the lower and upper states, respectively and the integral is the *transition moment*.

From the Born-Oppenheimer approximation, the wavefunctions can be separated into rotational, vibrational and electronic wavefunctions so that the total wavefunction is the product of these. Thus the total wavefunction can be written,

$$\psi = \psi_e(r, R)\psi_v(R)\psi_r(\theta, \phi), \tag{3}$$

where only the angular coordinates (θ, ϕ) are needed for the rotational wavefunction.

From here, the transition moment is now separable into radial and angular components. The square of the angular (rotational) component is the Hönl-London factor,

$$S_{J'J''} = \frac{1}{2J'' + 1} \left| \int \psi'^{*}_{r}\, \psi''_{r} \sin\theta \, d\theta d\phi \right|^2, \tag{4}$$

where a normalization factor has been included . An additional factor of $1/g$ is needed to address electronic degeneracies where $g = (2S + 1)(2 - \delta_{0,\Lambda' + \Lambda''})$. S and Λ are the spin and orbital angular momenta, respectively.

While the electronic and vibrational wavefunctions are both still functions of the inter-nuclear distance (R), the radial component can be further separated with the assumption that the electronic transitions occur much more rapidly than vibrational

transitions (the Franck-Condon principle). The integral over the vibrational wavefunctions is the *overlap integral*, the square of which is the Franck-Condon factor,

$$q_{v'v''} = \left| \int \psi'^{*}_{v} \psi''_{v} dR \right|^2, \tag{5}$$

The Franck-Condon factors are typically normalized such that $\sum_{v'} q_{v'v''} = 1$.

As a result, the total line strength can be expressed as the product of the electronic transition dipole moment and the Franck-Condon and Hönl-London factors,

$$S_{v'v''J'J''} = \left| \int \psi'^{*}_{e} \boldsymbol{\mu}_e \psi''_{e} d\boldsymbol{r} \right|^2 q_{v'v''} S_{J'J''}, \tag{6}$$

Of course, the electronic dipole transition moment is, strictly speaking, still a function of the internuclear separation, R, and is usually expressed in terms of so-called r-centroids that denote the most likely value of R at which the vibrational transition will occur [27, 28]. Contributions from different r-centroids were not specifically considered in the current analysis.

Finally, In order to compute the spectrum of a collection of molecules it is also necessary to consider the relative populations of molecules in the upper and lower states of the transitions. In thermodynamic equilibrium, the ratio of the number of molecules in the upper and lower states is given by the Boltzmann equation,

$$\frac{n'}{n''} = \frac{g'}{g''} \exp\left[- \left(E' - E'' \right) \Big/ k_B T \right], \tag{7}$$

where n is the number density in molecules per m^3, g is the statistical weight of the state (its degeneracy), E is the energy for the state, T is the temperature and k_B is the Boltzmann constant. For transitions from a manifold of upper states to a common lower state, this relationship can be written

$$n' = \frac{g'}{Q(T)} \mathrm{e}^{-E'/k_B T}, \tag{8}$$

where $Q(T)$ is the partition function defined as

$$Q(T) = \sum_j g_j \, \mathrm{e}^{-E_j/k_B T}. \tag{9}$$

2 EXPERIMENT

The original experiments to investigate effects of flame temperature on strontium molecular band shapes involved the injection of strontium compounds in solution into a methane-air flame, while spectra were recorded with a grating spectrometer. The laboratory setup, therefore, consisted of two principal components: 1) a CH_4-air burner apparatus fitted with a nebulizer for injecting the strontium solutions, and 2) a spectrometer consisting of a grating spectrograph fitted with a CCD photo-detector for acquiring digital spectra. In addition, a computer simulation has been designed for the current study to model specifically the SrO portions of the measured spectra for the purposes of flame diagnostics.

2.1 Burner Apparatus

Spectra were produced by injecting strontium-containing compounds in solution into a methane-air flame. Near-stoichiometric flames were produced with a 1x1-in Hencken burner supplied by laboratory air filtered through a Parker Standard Series 7F filter and ultra-high purity methane (99.97%) from Air Liquide America Specialty Gases. Flame temperature was modulated by holding the methane flow rate constant at 1.984-g/min while varying the flow of air. Gas and air flow rates were controlled using Edwards M-831 mass flow controllers

Direct measurement of the flame temperature was accomplished with a 1-mm diameter thermocouple inserted into the flame at 3-mm above the atomizer nozzle (center of the burner grid). Experiments were conducted at laboratory conditions (standard temperature and pressure) without pre-heating of the air, methane or solution.

Two different strontium-containing compounds were introduced into the methane-air flame. $SrCl_2$ and $Sr(OH)_2$ were each dissolved into distilled water at concentrations of 10-mg/mL and 2.5-mg/mL, respectively. A total of 12 experiments were performed: 6

experiments using the $Sr(OH)_2$ followed by 6 experiments using the $SrCl_2$. Since only one apparatus was available for the experimental investigations, the order of the experiments was chosen to avoid contaminating the $Sr(OH)_2$ doped flame with chlorine. Table 2-1 summarizes the thermocouple temperature measurements and air mass-flow rates.

The strontium compound solution was injected into the flame through a 0.052-in nozzle connected to a TSI-9302 atomizer set at 40-psi. The nozzle was mounted in the center of the burner grid for injection of the strontium solution directly into the flame. The strontium solution was injected at a mass-flow rate of 0.5-g/min.

Figure 2-1 shows an example of the strontium-compound-doped flame produced by the burner apparatus. The nebulizer nozzle is centered in the burner grid for direct injection. Not pictured is the thermocouple used to monitor flame temperature.

2.2 Spectrometer

Spectra were collected through a Czerny-Turner grating spectrograph using a simple, quartz imaging optical system with an approximate 5.0-degree field-of-view. With a 3 meter standoff distance from the spectrometer optics to the flame center, the entire flame was imaged onto the spectrometer slit. The spectrograph was configured with a 147-groove/mm grating and a 0.025-mm entrance slit. The spectra were focused onto a Princeton Instruments® PIXIS® detector with a 1340x100 pixel focal plane. The detector pixels were vertically binned and summed to result in an effective 1340x1 linear array which, when coupled with the 147-groove/mm grating and 0.025-mm slit, resulted in an estimated 0.408-nm/pixel spectral dispersion and a 3-pixel resolution of 1.22-nm at full-width-at-half-maximum (FWHM). The actual final resolution of the instrumented spectrometer system was determined from atomic line observations in the measured data as described in Section 3.3.

Table 2-1: Experiment Summary

Compound	Experiment Number	Air Flow Rate (l/min)	Temperature (°K)
Sr(OH)2	1	4.82	1488
	2	7.04	1553
	3	8.6	1623
	4	9.77	1593
	5	11.05	1628
	6	12.55	1643
SrCl2	7	4.48	1523
	8	6.95	1513
	9	9.29	1623
	10	11.55	1613
	11	13.04	1503
	12	14.05	1363

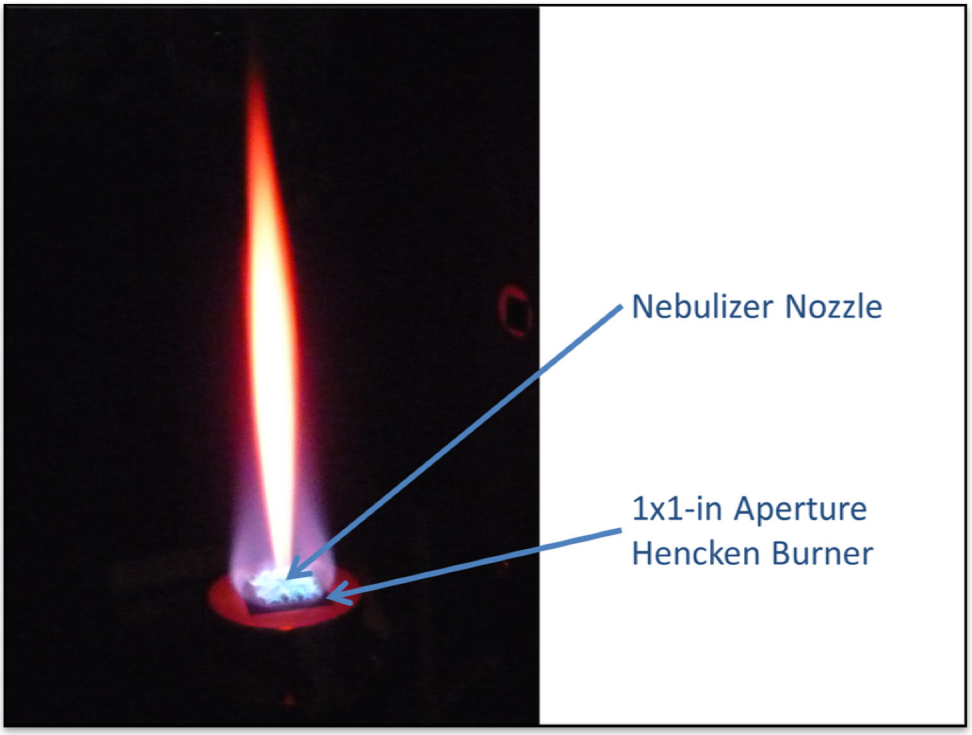


Figure 2-1: Burner apparatus.

The spectrometer was wavelength calibrated using a Pen-Ray® mercury atomic line source. Mercury atomic emission lines were identified to produce a wavelength calibration curve. Table 2-2 lists the lines identified from the mercury vapor source versus detector horizontal pixel number.

As can be seen from the calibration data, the mercury vapor lamp provided a sufficient number of observable lines to span the measured spectrum.

Table 2-2: Spectrometer Wavelength Calibration

Detector Pixel	Wavelength (nm)
147	404.656
223	435.833
490	546.073
565	576.96
570	579.066
1019	763.51
1137	811.531
1284	871.706

A National Instruments and Standards (NIST)-traceable, Optonic Laboratories Model 455, 6-in diameter integrating sphere with a 1-in aperture was used to calibrate the spectrometer system for spectral responsivity. Absolute radiometric spectral responsivity was calculated by collecting calibration lamp spectra at several luminosity settings. However, for the purposes of this study, spectra have been analyzed in terms of relative intensity.

2.3 Simulation

Spectra were simulated using PGOPHER [23], a freely available, open-source software package developed at the University of Bristol. PGOPHER is designed to simulate the rotational, vibrational and electronic spectra of gas-phase diatomic and linear-

polyatomic molecules as well as symmetric and asymmetric tops. PGOPHER is designed to run as a graphical user interface and, as such, the setup for complex simulations can be tedious. However, the input files are written in simple XML format and are easily editable with any basic text editor, which allows for some automation to be realized. As part of this work, a simple MatLab® routine was developed to construct the properly formatted input files with the desired parameters.

A variety of optional parameters are available in PGOPHER, however the primary focus was to assess the practical value for the current work. Consequently, PGOPHER was employed using primarily default inputs, which are designed to work for simple cases without further modification. Only the settings documented in this work were manipulated from the defaults making the model used as simple as possible while still addressing the relevant phenomena.

The structure of input parameters for PGOPHER follows a hierarchical format. The topmost object in the hierarchy is the *Simulation* object. This object stores settings for temperature, simulation units, *etc*. The *Species* object is below the simulation object. More than one species can be simulated simultaneously within PGOPHER by defining multiple *Species* objects. *Manifold* objects are below the *Species* objects. These objects represent a manifold of states and are useful for organizing related states (for example all of the vibrational states for a given electronic configuration). Finally, the S*tate* object is below the *Manifold* object. These objects define the specific states for which transitions are to be calculated. Settings for the S*tate* object include the electron orbital angular momentum (Sigma-, Sigma+, Pi…), state symmetry (gerade or ungerade) and electron spin (S). In addition, spectroscopic parameters are included at the state level such as the state origin, rotational constant, spin-orbit coupling constants, Lambda-doubling constants, *etc*.

Operationally, PGOPHER calculates a simulated spectrum as follows:

1) Calculate the energies and wavefunctions of the lower state.
2) Calculate the energies and wavefunctions of the upper state.
3) Calculate the transitions between states.

The energies and wavefunctions of the upper and lower states are computed from standard spectroscopic parameters. For heterogeneous diatomic molecules, only a few parameters are required for PGOPHER to generate representative rovibronic spectra. In particular, for a given state, besides the electronic angular momentum and spin, only a band origin and rotational constant (B_v) are required to produce rovibronic spectra. However, other spectroscopic constants to account for such effects as centrifugal distortion, lambda doubling and various momentum couplings are also supported.

For this study, band origins were derived from the standard polynomial expansion in powers of $(v+\frac{1}{2})$ [17],

$$T_{00} = \omega_e\left(v+\tfrac{1}{2}\right) - \omega_e x_e\left(v+\tfrac{1}{2}\right)^2 + \omega_e y_e\left(v+\tfrac{1}{2}\right)^3 + \cdots. \quad (10)$$

Likewise, the rotational constants (B_v) and, where available, centrifugal distortion constants (D_v) were derived as,

$$B_v = B_e - \alpha_e\left(v+\tfrac{1}{2}\right) + \gamma_e\left(v+\tfrac{1}{2}\right)^2 + \cdots, \quad (11)$$

$$D_v = D_e + \beta_e\left(v+\tfrac{1}{2}\right) + \cdots. \quad (12)$$

The most current Dunham constants available from the literature were used to derive the appropriate parameters. Table 2-3 summarizes the spectroscopic constants used to derive the PGOPHER input parameters.

Table 2-3: Spectroscopic constants for $^{88}Sr^{16}O$

Constant[1]	$X^1\Sigma^+$	$A^1\Sigma^+$	$A'^1\Pi$
ω_e	653.30998(140)	619.58	476.4327(1100)
$-\omega_e x_e$	-3.85078(79)	-0.89	-3.6114(890)
$\omega_e y_e$	-2.009(17)x10-2	-0.054	0.164(23)
$\omega_e z_e$	1.2837(160)x10-3	-	-0.005(1)
B_e	0.33797196(12)	0.30471	0.2572729(130)
$-\alpha_e$	-2.15598(22)x10-3	-0.00112	-2.4249(370)x10-3
γ_e	-1.9746(99)x10-5	-	0.2173(260)x10-3
$-D_e$	-3.61035(180)x10-7	-	-5.1924(540)x10-7
$-\beta_e$	-4.483(15)x10-9	-	2.045(100)x10-7

[1] Constants for $X^1\Sigma^+$ as reported by Li, et al. [10], constants for $A^1\Sigma^+$ and $A'^1\Pi$ as reported by Focsa, et al. [29]

Table 2-4: Spectroscopic constants for C_2

Constant[1]	$d^3\Pi_g$	$a^3\Pi_u$
ω_e	1788.52(33)	1641.3451(38)
$-\omega_e x_e$	-16.92(33)	-11.6583(14)
$\omega_e y_e$	-0.250(38)	-0.000888(122)
$\omega_e z_e$	-0.0401	-
B_e	1.755410(81)	1.632343(46)
$-\alpha_e$	-0.01960(12)	-0.016569(40)[a]
γ_e	-0.000141(38)	-0.0000294(61)
$-D_e$	-	-
$-\beta_e$	-	-

[1] Constants taken from Brooke and Bernath [30]

[a] The published value [30] was found to be in error by a factor of 100 as compared to previous work [31]. The corrected value was used.

PGOPHER is designed to compute transitions from the calculated upper and lower energy levels and wavefunctions. First, transition frequency is calculated from the energy differences. Transition intensities are then calculated from the transition dipole moments between the computed basis states. While customizations are available, the default operation of PGOPHER (and the one used herein) is to assume a standard Boltzmann distribution of states to compute relative intensities.

PGOPHER is designed to support calculation of transition moments in terms of the transition moment tensor. In this way, higher order moments (quadrupole, *etc.*) and multi-photon transitions can be supported. By default, however the transition tensor is assumed to have rank 1 so that only single photon, dipole transitions are considered. With these settings, the calculation of line strengths follows that of Section 1.4.

The XML formatted PGOPHER inputs for the simulated A-X transitions of SrO presented in this paper can be found in Appendix A. An additional PGOPHER model was constructed for diatomic carbon (see Section 3.4.2) the input file, for which, is given in Appendix B.

3 RESULTS AND DISCUSSION

The flame experiments show superposition spectra, in part due to complex chemistry and low spectral resolution. The spectra were surveyed to identify the most prominent atomic and molecular radiators. Rovibronic bands of the SrO A-X system were identified and subsequently isolated for analysis through a spectral differencing procedure. The SrO band system was then simulated and the results compared to the measured bands to determine flame thermodynamic properties. Finally, diatomic carbon emissions, also visible in some flames, were analyzed and the results compared to those of the SrO analysis.

3.1 Survey of Measured Spectra

Literature review made possible the identification of most of the atomic and molecular structure observed in the experimental spectra. Figure 3-1 shows a survey of the species identified in the flame spectra for both of the compounds studied.

Atomic lines observed in the flame spectra were identified from the NIST Atomic Spectral Database [32]. The prominent strontium atomic line at 460.7-nm is clearly attributable to the experimental compounds used. Sodium and potassium lines are also visible in the measured spectra of both of the experimental compounds.

Identification of molecular species was somewhat more involved. First, the NASA Chemical Equilibrium with Applications (CEA) code was used to predict the products of combustion for the experimental flame compositions [15]. Literature search was then performed for the species with the highest predicted concentrations in an attempt to identify as many spectral constituents as possible. Example CEA results for an $SrCl_2$ doped flame at 1613-K are shown in Table 3-1 (the complete output file is shown in Appendix C).

The most intense molecular bands in Figure 3-1 occur in the region between 600-nm and 700-nm and are attributable to the SrOH, $A - X$ and $B - X$ transitions [8, 33]. The CH $A - X$ and $B - X$ bands and C_2 Swan bands [16], typical of hydrocarbon-air combustion, are also clearly visible in the region from about 380-nm to 580-nm. Also observable in this region is an apparent, red-degraded continuum, which has been attributed to chemiluminescence from reactions like $CO + O \rightarrow CO_2 + h\nu$ [34, 35]. Finally, $A - X$ transition bands for SrO [11] are clearly observed in the spectrum of the $SrCl_2$ solution underlain by two bands that could not be identified. The unidentified bands, however, can be seen most clearly in the spectra of the $Sr(OH)_2$ solution due to the extremely low contribution from the SrO $A - X$ bands in the $Sr(OH)_2$ spectra.

Noticeably absent from the measured spectra are the hydrogen atomic lines (e.g. the Balmer series α, β, γ, etc.) as well as atomic lines of argon and chlorine, all species predicted to occur in significant abundance in the flame (Table 3-1).

3.2 SrO Formation and Emissions

As previously stated, the molecular species of specific interest to this study is strontium monoxide. In particular, the $A^1\Sigma^+ - X^1\Sigma^+$ bands for four vibrational transitions can be clearly identified in the spectra of the $SrCl_2$ solution in Figure 3-1. Band heads are visible at around 750-nm, 790-nm, 830-nm and 870-nm with the bands degraded toward the red end of the spectrum.

From the observed spectra, SrO concentration appears to be much higher in the $SrCl_2$-doped flame than in the $Sr(OH)_2$ flame. Increased SrO formation in chlorinated strontium flames has, in fact, been documented in studies related to pyrotechnic color enhancement [36, 37]. One possible explanation is related to the availability of free strontium in the flame due to the dissociation of Sr-Cl bonds.

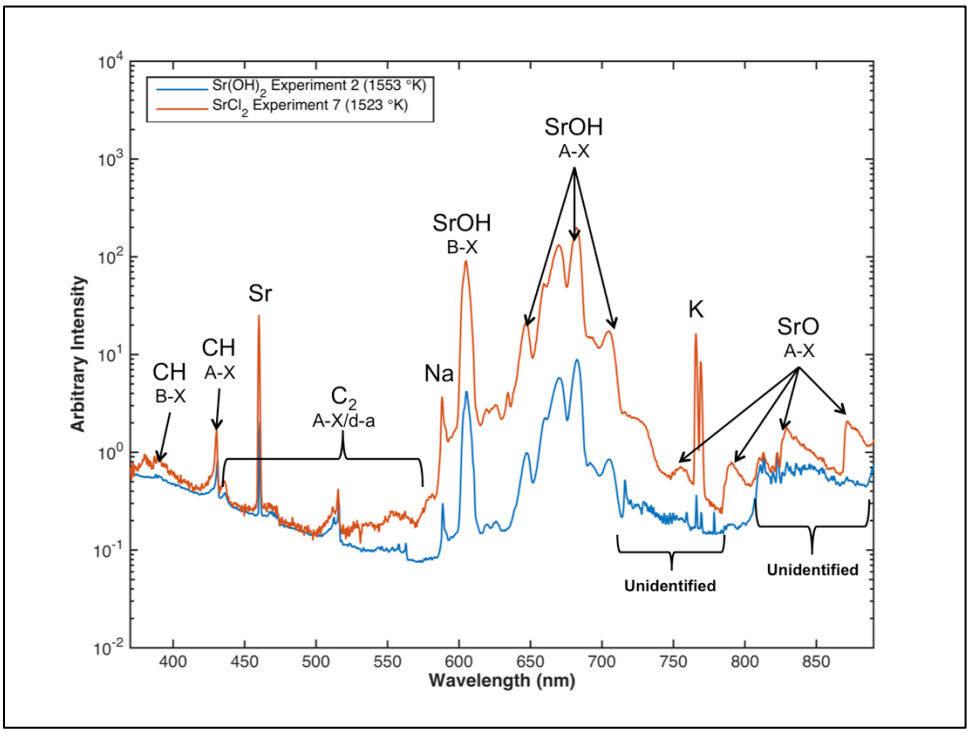


Figure 3-1: Survey of species in experimental spectra.

Table 3-1: Example CEA results for $SrCl_2$-doped flame at 1613-K

Molecular Species	Mass Fraction[1]	Molecular Species	Mass Fraction[1]
*Ar	1.1316E-02	H_2O	1.3993E-01
CH_4	5.0440E-10	NH_2	4.5960E-10
*CO	9.3095E-02	NH_3	9.0551E-07
*CO_2	8.0751E-02	*NO	6.1088E-08
COOH	9.3920E-10	*N_2	6.6162E-01
*Cl	1.8079E-07	*O	1.4420E-10
*H	8.6290E-07	*OH	1.1647E-06
HCN	2.8018E-08	*O_2	2.2200E-10
HCO	2.1012E-09	*Sr	3.6499E-09
HCl	1.2689E-03	*SrCl	5.7311E-07
HNC	5.7430E-10	$SrCL_2$	9.4065E-04
HNCO	2.2008E-08	*SrO	2.6350E-10
*H_2	9.2716E-03	SrOH	2.4006E-07
HCHO, formaldehyde	4.8835E-09	$Sr(OH)_2$	5.5707E-05
HCOOH	1.3550E-08	SrO(cr)	1.7554E-03

* Thermodynamic Properties Fitted To 20000-K (per CEA output)
[1] Mass fractions below 1E-10 were considered trace species for this example
(cr) indicates solid phase, no designation indicates gas phase

SrO is formed primarily when atomic strontium combines with oxygen,

$$2Sr + O_2 \rightarrow 2SrO.$$

Therefore, the availability of free strontium atoms in the flame is the principal driver for the formation of SrO (as molecular oxygen is readily available from both atmospheric and supply air). A cursory analysis of the relative bond dissociation energies for the relevant species gives some insight into the preferential formation of SrO in the $SrCl_2$ flame. Table 3-2 shows that, among the relevant species, the lowest bond dissociation energy belongs to the Sr-Cl bond in strontium monochloride (SrCl). As SrCl is formed from $SrCl_2$ breakdown, it quickly dissociates producing the free strontium needed for SrO formation.

Table 3-2: Dissociation energies of strontium molecular bonds

Bond[1]	Reaction	Dissociation Energy at 0K (kJ/mol)
Sr-O	$SrO \rightarrow Sr + O$	460 ±64
	$SrOH \rightarrow Sr + OH$	410 ±64
	$Sr(OH)_2 \rightarrow SrOH + OH$	490 ±113
Sr-Cl	$SrCl \rightarrow Sr + Cl$	335 ±84
	$SrCl_2 \rightarrow SrCl + Cl$	418 ±25

[1] Data taken from Stans, et al. [38]

SrO is expected to occur inside the flame in multiple phases simultaneously (see Table 3-1). This fact has some subtle but important implications with respect to the rovibronic emissions observed in the flame. While diatomic molecules in the gas phase tend to show well-quantized rovibronic fine structure, molecules in condensed phases may not [17, 39]. In condensed phases, rotational degrees of freedom are limited by molecular interactions or rotation is suppressed entirely causing rotational fine structure to degrade or disappear. Vibrational states, on the other hand, tend to be less affected

and often result in only small shifts to the observed vibrational spectra. Nevertheless, the combined effect of rotational and vibrational state perturbations attributable to the presence of solid or liquid SrO in the flame could further decrease the resolution of the rovibronic band structure.

3.3 Simulated Spectra

In order to compare simulation results to the observed SrO emissions, the SrO bands were isolated by subtraction of the underlying spectral shape. SrO A-X emissions in the spectra of the $SrCl_2$ flames were isolated by careful subtraction of the underlying spectra provided by the $Sr(OH)_2$ flames. An example SrO-isolated spectrum is shown in Figure 3-2. The SrO $A^1\Sigma^+ - X^1\Sigma^+$ vibrational transitions for $\Delta v = 1,2,3,4$ are relatively easily identifiable after subtraction of the underlying spectral shape.

Of course, the spectral differencing approach used assumes that the $Sr(OH)_2$ spectrum contains a subset of the emissions present in the $SrCl_2$ spectrum, at least in the spectral region of interest. Likewise, the flame is assumed to be optically thin so that the spectra of different radiators are additive. Non-negligible optical thickness and differences in the relative concentrations of emitting species, the underlying incandescent radiation and the thermodynamic conditions in the flames could all result in differencing artifacts in the SrO-isolated spectra. Nevertheless, the degree to which these differences can be neglected and the above assumptions hold is borne out in the results. Confirmation of the assumptions of the differencing approach should be evident when the SrO-isolated spectra are compared to the simulated (idealized) spectra.

Using PGOPHER, SrO $A^1\Sigma^+ - X^1\Sigma^+$ rovibronic transitions were modeled for vibrational states up to $v = 10$ for both the upper and lower electronic states and rotational states out to $J_{max} = 200$. The computed line spectra (line positions and intensities without broadening) for the $\Delta v = 1,2,3,4$ rovibronic bands as simulated at 1613-K are shown in Figure 3-3.

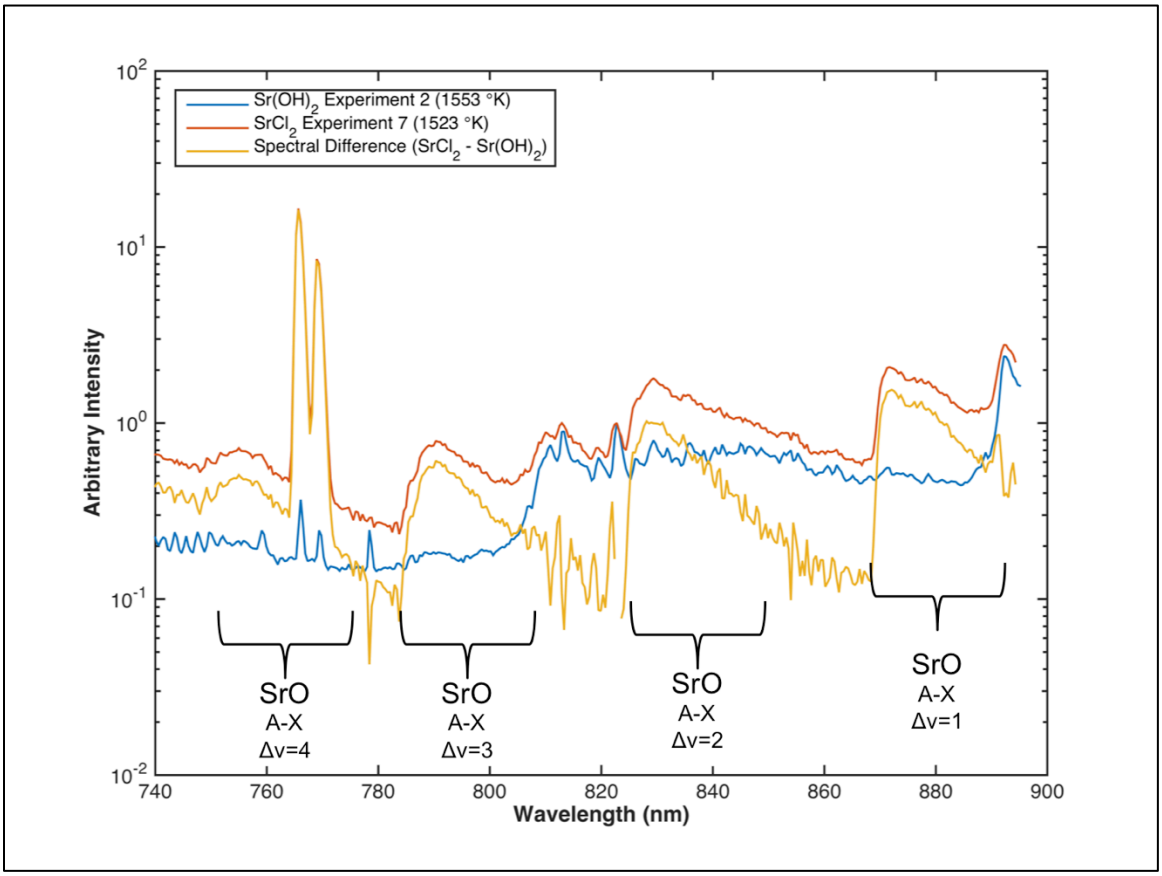


Figure 3-2: SrO-isolated spectrum.

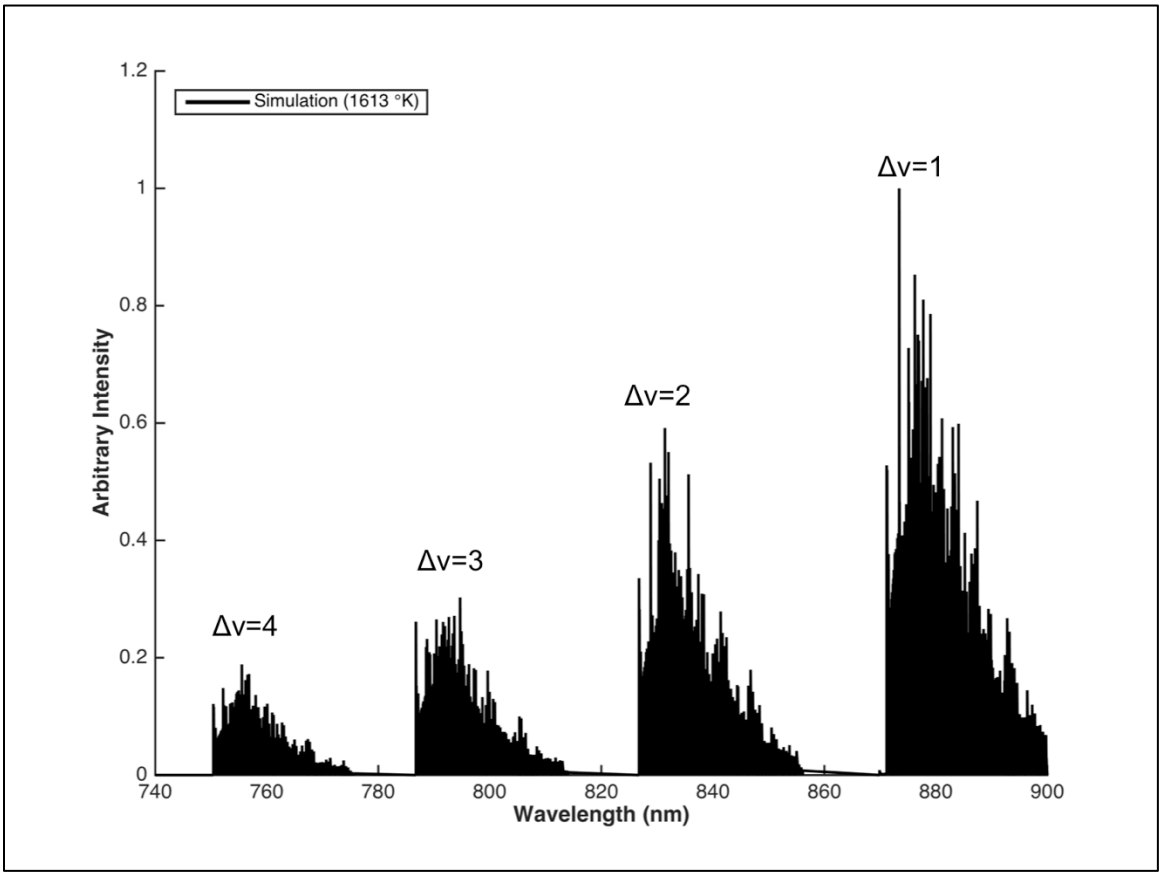


Figure 3-3: Simulated relative line strengths of the SrO $A^1\Sigma^+$-$X^1\Sigma^+$ band system.

The instrumental effects of the spectrometer-detector system were simulated with the Gaussian facility in PGOPHER. PGOPHER allows one to model both Gaussian and Lorentzian line shape effects. While these can be used to simulate various line-broadening effects such as pressure and/or Doppler broadening, only the instrumental effects were simulated for this study. Doppler broadening, for example, is related to the flame temperature by

$$\Delta\nu_{FWHM} = \nu_0 \sqrt{\frac{8\ln(2)\, k_B T}{mc^2}}, \tag{13}$$

where m is the mass, T is the flame temperature and c is the speed of light. The FWHM for Doppler broadening is then on the order of 10^{-5}-nm for atomic Sr and 10^{-4}-nm for SrO in the temperature range measured.

The Sr I atomic line at 460.7-nm was used to determine the effective resolution of the system (Figure 3-4). The Sr I atomic line in the measured spectrum was found to have an apparent line width of 0.82-nm at full-width-half-maximum. Since instrumental effects dominate the measured strontium atomic line shapes, a value of 0.8-nm was used as the Gaussian FWHM in the simulations. Figure 3-5 shows the resulting, line-broadened simulation compared to SrO-isolated spectra for two of the experimental trials.

The simulated spectrum in Figure 3-5 significantly under predicts the measurement in the $\Delta v = 4$ band region. This is most likely attributable to underlying spectral shape not completely removed by spectral differencing. The simulated results for the remaining bands, $\Delta v = 1,2,3$, appear to follow the overall shape of the rotational-vibrational distributions closely. However, differences still exist in the rotational structure of some bands particularly in the band head regions. The band head differences are most noticeable in the $\Delta v = 1$ band and to a lesser extent the $\Delta v = 2$ band.

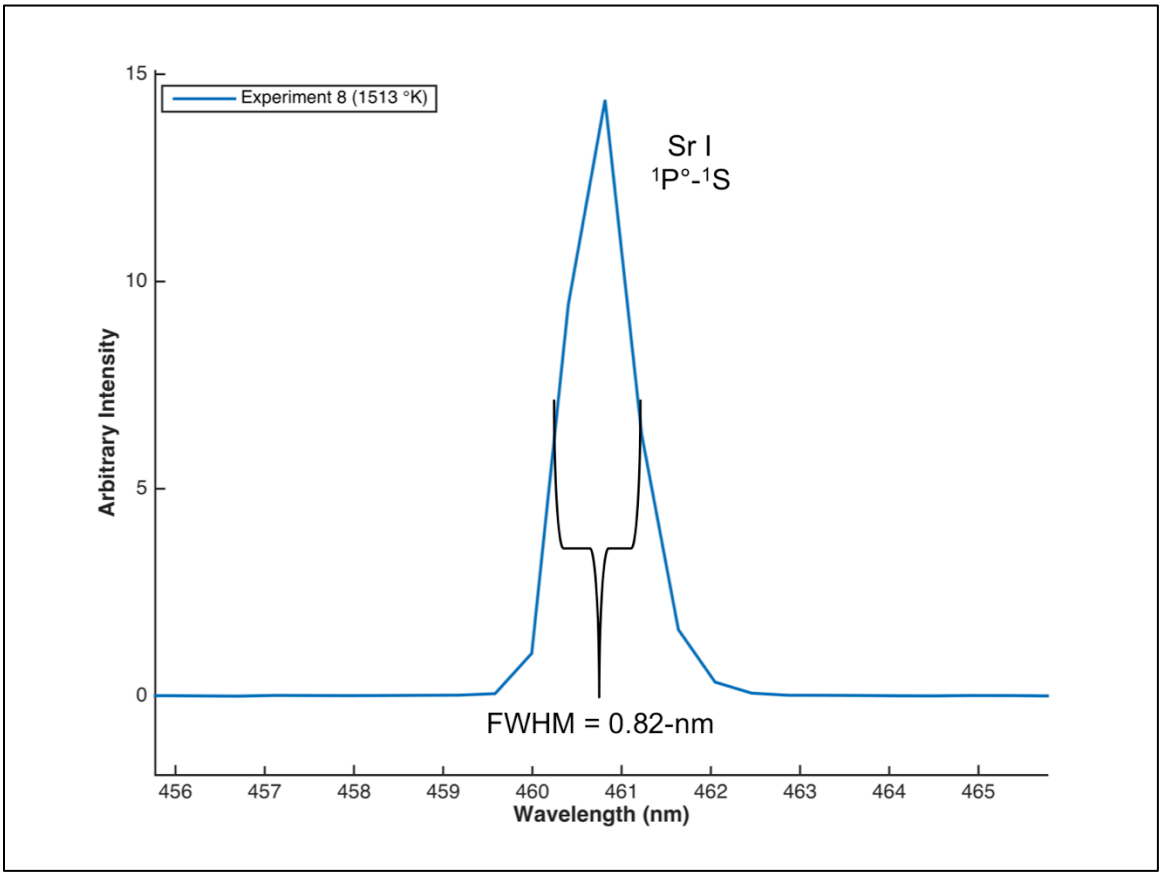


Figure 3-4: Spectrometer resolution determined from Sr I atomic line.

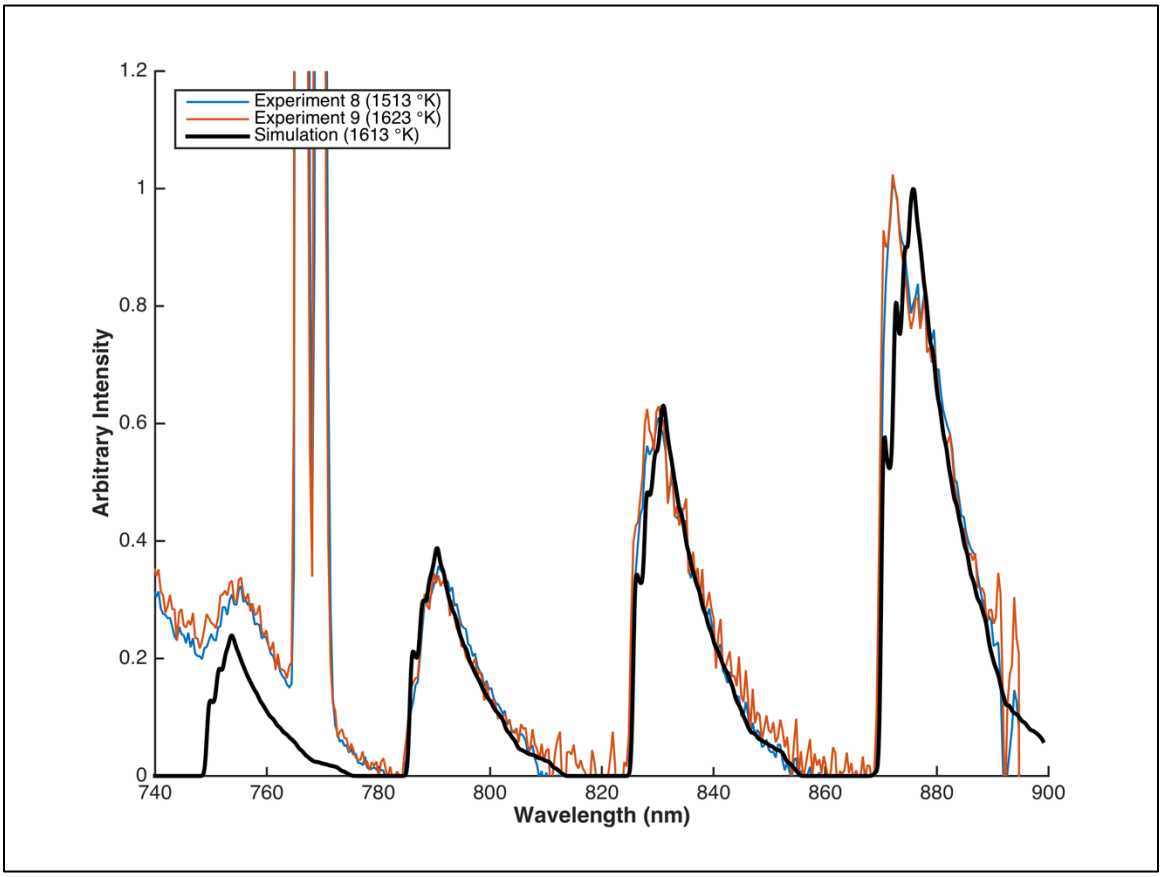


Figure 3-5: SrO A-X system: Simulated versus recorded spectra.

Several factors could be responsible for the differences observed between the simulated and measured band head shapes. First, the simulation only includes a single isotopologue of SrO, namely, $^{88}Sr^{16}O$. Four stable isotopes of strontium exist with three in significant abundance: ^{88}Sr (82.58%), ^{87}Sr (7.0%) and ^{86}Sr (9.86%) [40]. Isotopologues of SrO for each of these are therefore expected in the experimental flame in similar relative abundance.

Study of isotopologic shifts of SrO vibrational bands has revealed that the A-X band heads can shift by as much as 0.4-nm [11]. Therefore, inclusion of other isotopologues in the simulation would affect primarily the shape of the band head region of the vibronic bands and may therefore produce somewhat better agreement with the measured shape. The characterization of the occurrences and concentrations of isotopologues may be of future interest and can be viewed as an extension of the current work.

More likely, however, the band head shape differences are an indication of temperature inhomogeneity within the flame, as discussed in more detail in Section 3.4. The current simulation allows one to specify one temperature. For that reason, the simulated spectra represent an effectively homogenous temperature distribution throughout the flame. A possible further refinement would be to simulate several SrO populations each with an independent temperature and concentration, subsequently; variations can be implemented to find a better fit to the measured spectral shape.

Other electronic transitions of SrO were also considered as possible contributors to the observed band head shapes. Although the additional transitions did not reproduce the band head features observed, some of the fine structure of the measured bands could be explained in this way. While several of the fine details appear to be due to artifacts resulting from spectral differencing, certain features appear repeatable. Figure 3-6 shows the result of averaging the SrO-isolated spectra for two trials in the $\Delta v = 3$ band (blue line). By averaging recoded data, repeatable features are enhanced and noise and differencing artifacts are diminished.

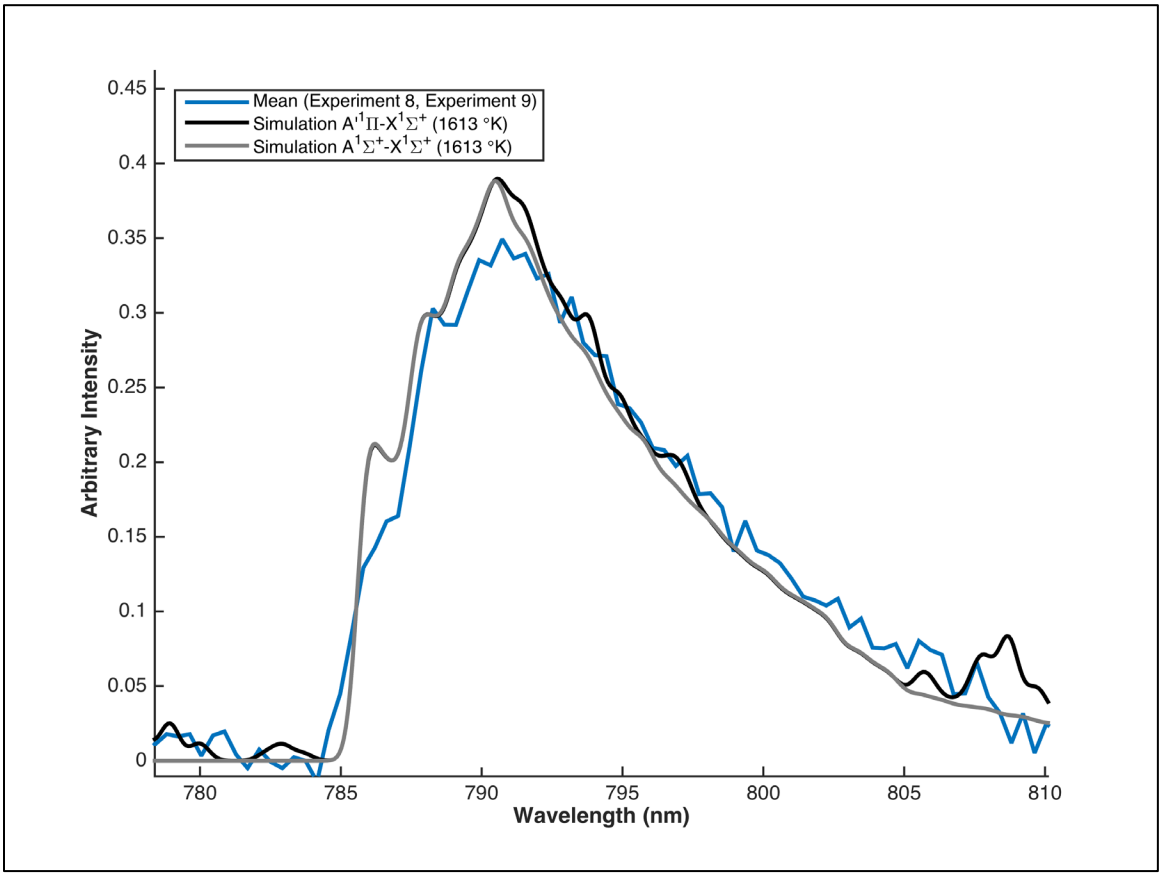


Figure 3-6: Effect of additional state transitions on simulated spectra.

Also shown in Figure 3-6 are simulations for the $\Sigma - \Sigma$ transition (gray) and a superposition of the $\Sigma - \Sigma$ band with contributions from the SrO $\Pi - \Sigma$ system (black). Comparisons of the band heads between the two simulations indicate insignificant changes in shape; however, when additional electronic transitions are considered, additional features do appear in the band tail.

For the purposes of this study, the $\Sigma - \Sigma$ transitions were specifically of interest since the overall contributions from fine-detail variations are relatively small. With only the indicated refinements, however, the simulations already appear to follow more closely to portions of the repeatable structure seen in the measured spectra. Future study may be able to isolate the sources of the fine-detail variations.

3.4 Flame Diagnostics

By default, PGOPHER assumes a condition of local thermodynamic equilibrium when computing relative line strengths. When given a rotational temperature, T_{rot}, PGOPHER assumes the same vibrational temperature, T_{vib}, unless otherwise specified. Likewise, when computing normalized relative spectral intensity, the energy distribution among states for the simulated spectra obeys a Boltzmann distribution. Specifically, PGOPHER allows one to compute the normalized intensity as

$$I_{norm} = \frac{S}{Q}\left[\exp\left(\frac{-E_{lower}}{k_B T}\right) - \exp\left(\frac{-E_{upper}}{k_B T}\right)\right], \tag{14}$$

$$Q = \sum g e^{-E k_B T}, \tag{15}$$

where S is the line strength and Q is the partition function[1]. The extent to which the measured intensity distributions match the simulations is an indication of a condition of LTE in the flame. More precisely, LTE implies that $T = T_{rot} = T_{vib}$ where T also equals the flame temperature that was measured by thermocouple.

3.4.1 SrO A-X Bands

From Figure 3-5, it is clear that the simulated distribution of intensities for SrO matches well with measurements in a gross sense indicating strong support for the assumption of LTE in the flame.

It is noteworthy that the measured flame temperatures for the experimental results displayed in Figure 3-5 differ by 110-K, yet the measured spectral distributions are nearly identical. In fact, as seen in Figure 3-7, all of the $SrCl_2$ experiments show similar distributions (note that experiments 11 and 12 are not included due to low signal-to-noise). For comparison, these spectra were normalized to the value of the peak intensity at the $\Delta v = 1$ band head. The most significant differences are seen in the higher vibrational transitions ($\Delta v = 3,4$). This behavior should be expected of flames in LTE but at different temperatures since higher energy states are more sensitive to changes in temperature.

However, the expected trend of increasing band intensity with increasing temperature requires further discussion in view of the measured data. Looking closely at the $\Delta v = 3$ band in Figure 3-8, it appears that the relative intensity of the band is lower for the experiment at 1623-K than for the experiment at 1513-K. For reference, simulations at 1513-K and 1613-K are also shown and clearly demonstrate the expected trend in intensity versus temperature. While the unexpected trend in the measured spectra could be an artifact of the spectral differencing procedure, the same behavior can be

[1] The sum in the partition function is taken over all manifolds in the upper state when simulating emission spectra. Q is defined such that the populations sum to unity.

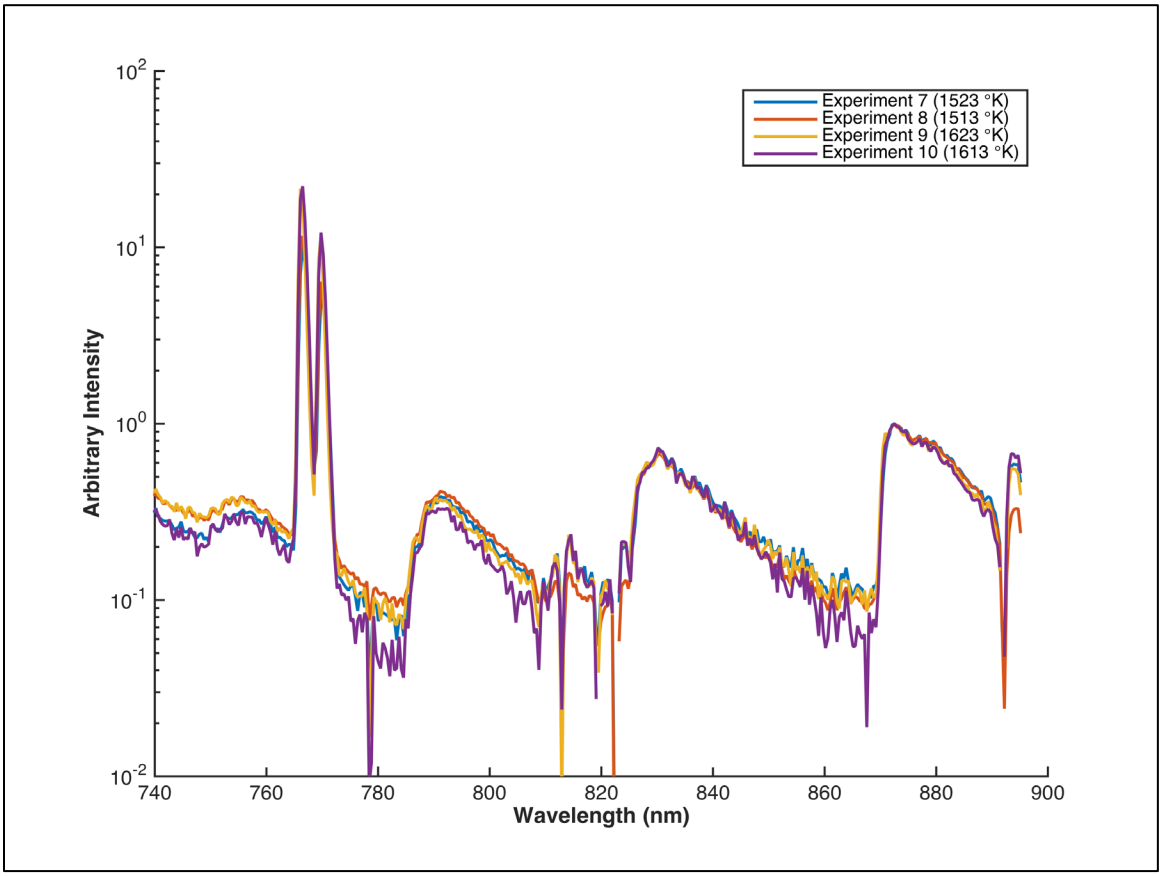


Figure 3-7: SrO A-X system in experiments 7-10, normalized to the $\Delta v = 1$ band head signals.

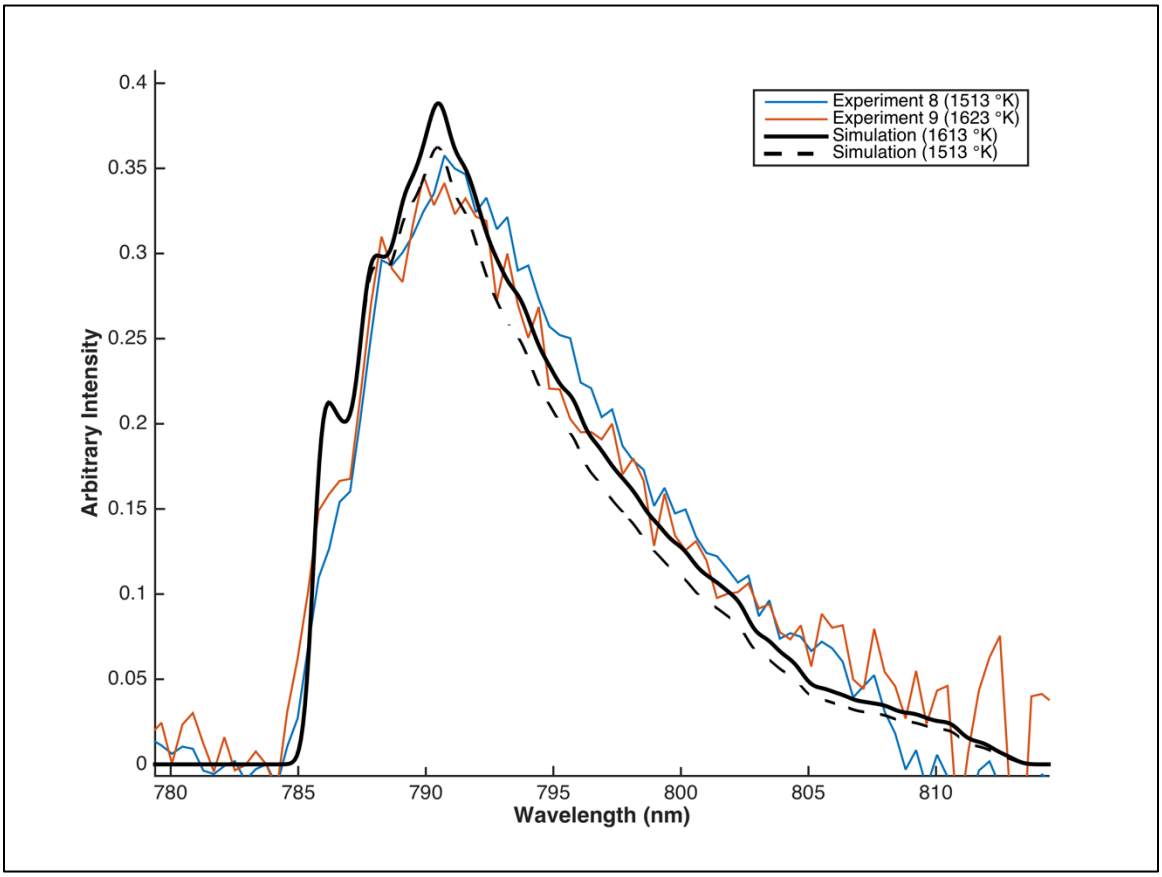


Figure 3-8: Temperature trends in the measured SrO $\Delta v = 3$ band.

explained by an inhomogeneous temperature distribution within the flame. As previously stated, higher energy bands are more sensitive to temperature. As a result, small differences in temperature distribution from flame to flame could easily explain the observed differences in the relative band intensities. Furthermore, inhomogeneity of flame temperature could also explain the observed band head shapes. Figure 3-9 shows a measured spectrum compared to simulations at three different temperatures (800-K, 1613-K, and 2200-K).

The shape of the $\Delta v = 1$ band head illustrated in Figure 3-9 most closely matches the low temperature (800-K) spectral simulation whereas the tail of the band most closely approaches the simulation at the experimental temperature (1613-K). The other bands show a similar, albeit less pronounced behavior near the band head but more clearly adhere to the shape of the 1613-K simulation indicating that the high temperature (2200-K) simulation is decidedly not a good fit. This behavior suggests that the flame may actually show a distribution of temperatures bounded above by the temperature measured at the thermocouple.

3.4.2 C_2 Swan Band

Observations of the C_2 Swan bands were available in some of the measured spectra which afforded the opportunity to verify the flame temperature and LTE condition independently from the SrO band system. PGOPHER was again used to simulate the most observable transition of the C_2 system, namely the $\Delta v = 0$ band of the $d^3\Pi_g - a^3\Pi_u$ transition. Spectroscopic constants used for the C_2 simulation are given in Table 2-4. As with the SrO simulation, isotopologues of C_2 were not considered.

Simulated and measured spectra for the C_2 $\Delta v = 0$ band are shown in Figure 3-10 for two temperatures. For these comparisons, instead of the differencing technique used above, a simple linear correction was applied to the measured spectra to remove the underlying continuum background.

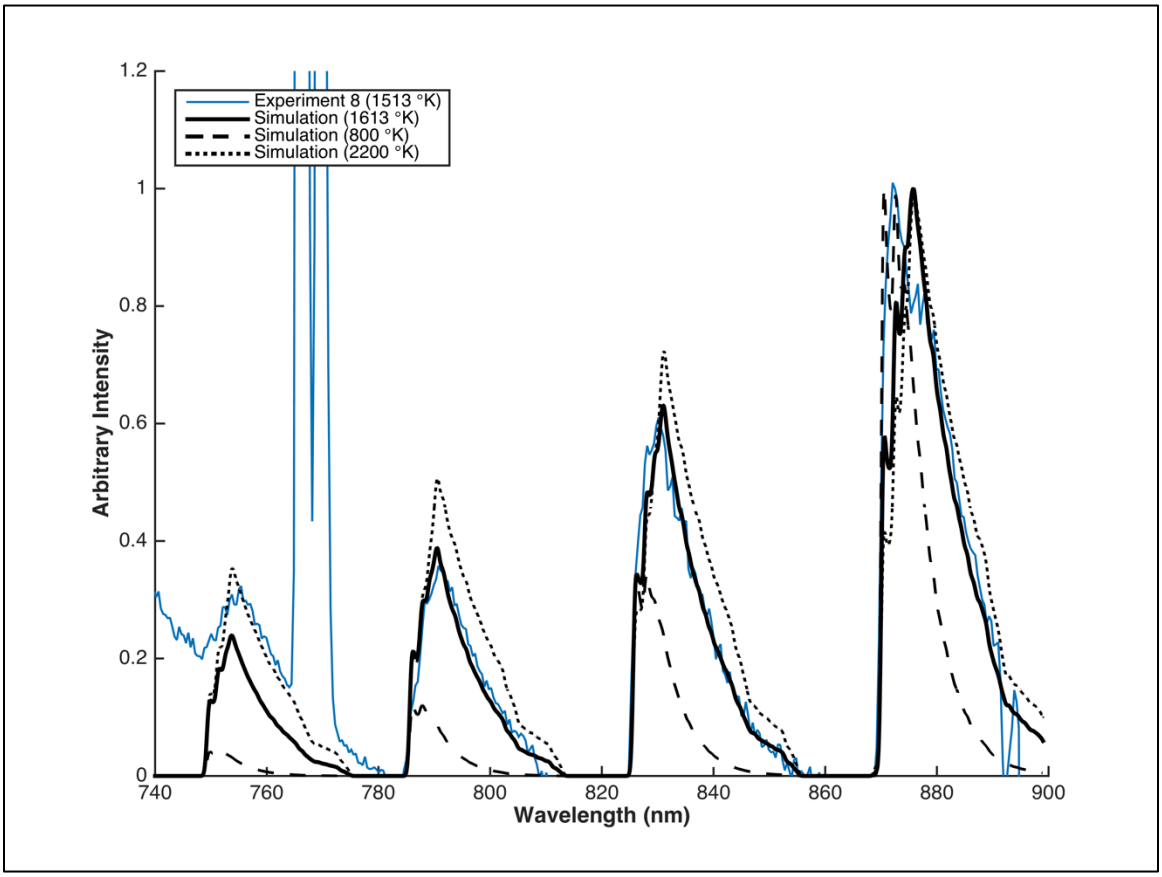


Figure 3-9: Effect of temperature on the band head shape.

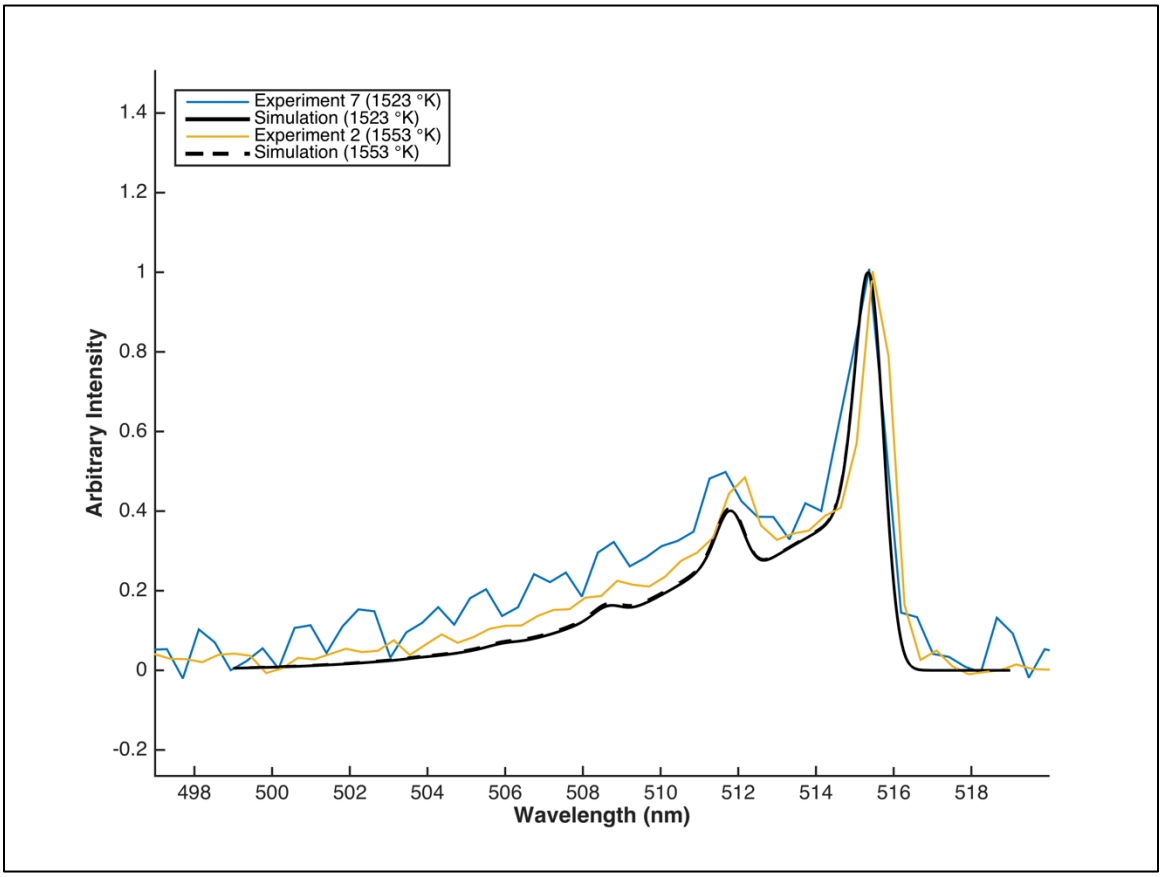


Figure 3-10: C_2 d-a $\Delta v = 0$: Simulated versus recorded spectra.

In Figure 3-10, the $Sr(OH)_2$ trial (Experiment 2) matches the simulated spectrum more closely than the $SrCl_2$ trial (Experiment 7) due to a change in spectrometer sensitivity settings that decreased the signal-to-noise ratio in the $SrCl_2$ experiments. Nevertheless, the comparisons of measurements to simulations in this band again indicate reasonable agreement between the diatomic emissions and the thermocouple readings as well as further supporting the assumption of LTE. Similar results were also achieved using the Nelder-Mead Temperature program [21] (see Appendix D).

4 CONCLUSIONS AND RECOMMENDATIONS

This study has demonstrated that the recorded data can be simulated with PGOPHER. The overall spectral shapes seen in the data are reproduced with a simulation temperature within ±7% to that measured by a thermocouple. Moreover, the spectral shape observed in the SrO-isolated spectra supports the assumption of LTE. The observed distributions of band intensities as well as the rotational shapes of the bands are both indications that SrO is in LTE in the measured spectra. The assumption of an optically thin flame, upon which the spectral differencing procedure was based, is also supported by the close match between the simulated and SrO-isolated spectra.

The principal discrepancies observed between the measurements and simulations occur in the band head regions of the low energy vibronic transitions. Two possible explanations for these differences are suggested, namely, isotopologic band head shift and inhomogeneous temperature distribution in the flame. While the effect of isotopologues on band head shape is expected to be small, the effect of inhomogeneity of flame temperature can be potentially significant.

Additional analysis can be accomplished for the recorded diatomic carbon emissions that are discernible in the flame spectra. Measured signatures from the C_2 Swan band support the hypothesis of LTE in the flame. The determined spectroscopic temperatures are in reasonable agreement with the results obtained from thermocouple and the simulated SrO spectra. In turn, the C_2 Swan studies add further support to the results from the analysis of the SrO spectra.

PGOPHER is capable of more sophisticated diatomic simulations than the ones implemented for this study. Consideration of additional electronic state transitions, for example, beyond the single SrO $\Sigma - \Sigma$ transition modeled here, and addition of isotopologues could both potentially improve the quality of fit to data. Likewise, PGOPHER is capable of contour fitting to measurements while allowing parameters,

such as temperature, to float as variables. Future efforts may be able to leverage this capability to further refine the estimated temperature.

Future measurements of SrO in the near-infrared region of methane-air flames could also improve the understanding of the flame conditions. Increased spectral resolution could potentially resolve the rotational structure of the bands making conventional techniques, like Boltzmann plots, more viable. At the same time, the spectrometer used for these experiments is capable of imaging along the slit dimension making measurements of variations in spectral distribution possible in at least one dimension. Using the methods presented in this study is expected to allow one to estimate the flame temperature distribution along the imaged dimension.

Finally, further literature review may lead to the identification of the as yet unidentified spectral features observed in the NIR region concurrent with the SrO emissions. Identification of these features could enable improved spectral differencing or perhaps spectral modeling of additional species.

REFERENCES

[1] K. Kenmochi, V. Ann Dinh, K. Sato, A. Yanase, H. Katayama-Yoshida, Materials Design of Transparent and Half-Metallic Ferromagnets of MgO, SrO and BaO without Magnetic Elements, Journal of the Physical Society of Japan 73 (2004) 2952-2954.

[2] T. Seki, K. Akutsu, H. Hattori, Calcium oxide and strontium oxide as environmentally benign and highly efficient heterogeneous catalysts for the Tishchenko reaction of furfural, Chem Commun (Camb) (2001) 1000-1001.

[3] S.S. Banerjee, S. Tarafder, N.M. Davies, A. Bandyopadhyay, S. Bose, Understanding the influence of MgO and SrO binary doping on the mechanical and biological properties of β-TCP ceramics, Acta Biomaterialia 6 (2010) 4167-4174.

[4] W. Meyerriecks, K.L. Kosanke, Color Values and Spectra of the Principal Emitters in Colored Flames, J. Pyrotechnics 18 (2003) 1-22.

[5] R.S. Ram, K. Tereszchuk, K.A. Walker, P.F. Bernath, High resolution emission spectroscopy of the $E^2\Pi$–$X^2\Sigma^+$ transition of SrH and SrD, J Mol Spectrosc 271 (2012) 15-19.

[6] M.S. Beardah, A.M. Ellis, Observation of a new transition of the SrOH free radical, J Mol Spectrosc 218 (2003) 80-84.

[7] C.R. Brazier, P.F. Bernath, Laser and fourier transform spectroscopy of the $\tilde{A}^2\Pi$ -$\tilde{X}^2\Sigma^+$ transition of SrOH, J Mol Spectrosc 114 (1985) 163-173.

[8] H.G.C. Human, P.J.T. Zeegers, Molecular fluorescence of CaOH, SrOH and BaCl in flames, Spectrochimica Acta Part B: Atomic Spectroscopy 30 (1975) 203-209.

[9] R.F.W. Herrmann, G.K. Sumnicht, M. Stein, W.E. Ernst, The orange band system of SrO: First details about the triplet transitions, J Mol Spectrosc 156 (1992) 487-500.

[10] H. Li, R. Skelton, C. Focsa, B. Pinchemel, P.F. Bernath, Fourier Transform Spectroscopy of Chemiluminescence from the SrO $A^1\Sigma^+$-$X^1\Sigma^+$ Transition, J Mol Spectrosc 203 (2000) 188-195.

[11] X.L. Mao, A.A. Bol'shakov, I. Choi, C.P. McKay, D.L. Perry, O. Sorkhabi, R.E. Russo, Laser Ablation Molecular Isotopic Spectrometry: Strontium and its isotopes, Spectrochimica Acta Part B-Atomic Spectroscopy 66 (2011) 767-775.

[12] D.A. Cremers, L.J. Radziemski, Handbook of Laser-Induced Breakdown Spectroscopy, 2nd Edition (Blackwell Science Publ, Oxford, 2013).

[13] J.G. Wang, P.M. Sheridan, M.J. Dick, P.F. Bernath, Optical-optical double-resonance spectroscopy of SrOH: The $\tilde{C}^2\Pi(000)$-$\tilde{A}^2\Pi(000)$ transition, J Mol Spectrosc 236 (2006) 21-28.

[14] R. Marvodineanu, H. Boiteux, R. Mavrodineanu, Flame Spectroscopy, 1965).

[15] B.P. Herndon, Characterization of SrOH in a Methane Air Flame, (University of Tennessee Space Institute, 2012).

[16] A.K. Sandrowitz, J.M. Cooke, N.G. Glumac, Flame emission spectroscopy for equivalence ratio monitoring, Applied Spectroscopy 52 (1998) 658-662.

[17] G. Herzberg, Molecular spectra and molecular structure (R.E. Krieger Pub. Co., Malabar, Fla., 1989).

[18] A. Thorne, U. Litzén, S. Johansson, Spectrophysics: Principles and Applications (Springer Science & Business Media, 1999).

[19] C.G. Parigger, Atomic and molecular emissions in laser-induced breakdown spectroscopy, Spectrochimica Acta Part B: Atomic Spectroscopy 79–80 4-16.

[20] J.O. Hornkohl, C. Parigger, J.W.L. Lewis, Temperature measurements from CN spectra in a laser-induced plasma, Journal of Quantitative Spectroscopy and Radiative Transfer 46 (1991) 405-411.

[21] C.G. Parigger, A.C. Woods, D.M. Surmick, G. Gautam, M.J. Witte, J.O. Hornkohl, Computation of diatomic molecular spectra for selected transitions of aluminum monoxide, cyanide, diatomic carbon, and titanium monoxide, Spectrochimica Acta Part B: Atomic Spectroscopy 107 (2015) 132-138.

[22] A.F.H. van Gessel, B. Hrycak, M. Jasinski, J. Mizeraczyk, J. van der Mullen, P.J. Bruggeman, Temperature fitting of partially resolved rotational spectra, Journal of Instrumentation 7 (2012) 9.

[23] PGOPHER, version 8.0, C.M. Western, 2014, University of Bristol Research Data Repository, doi:10.5523/bris.huflggvpcuc1zvliqed497r2

[24] J.M. Hollas, Modern spectroscopy (J. Wiley, Chichester ; Hoboken, NJ, 2004).

[25] P.F. Bernath, Spectra of Atoms and Molecules (Oxford University Press, 2005).

[26] B.H. Bransden, C.J. Joachain, Physics of Atoms and Molecules (Pearson Education, 2006).

[27] B. Karthikeyan, V. Raja, N. Rajamanickam, S. Bagare, On the Franck-Condon factors and R-centroids of the astrophysically interesting molecule CS, Serbian Astronomical Journal 175 (2007) 25-32.

[28] S. Yazykova, E. Butyrskaya, Mathematical justification of the r-centroid method in diatomic molecules, Journal of Physics B: Atomic and Molecular Physics 13 (1980) 3361.

[29] C. Focsa, A. Poclet, B. Pinchemel, R.J. Le Roy, P.F. Bernath, Fourier Transform Spectroscopy of the $A'^1\Pi$-$X^1\Sigma^+$ System of CaO, J Mol Spectrosc 203 (2000) 330-338.

[30] J.S.A. Brooke, P.F. Bernath, T.W. Schmidt, G.B. Bacskay, Line strengths and updated molecular constants for the C_2 Swan system, Journal of Quantitative Spectroscopy & Radiative Transfer 124 (2013) 11-20.

[31] C.V.V. Prasad, P.F. Bernath, Fourier-Transform Spectroscopy of the Swan $d^3\Pi_g$-$A^3\Pi_u$ System of the Jet-Cooled C_2 Molecule, Astrophysical Journal 426 (1994) 812-821.

[32] A. Kramida, Ralchenko, Yu., Reader, J. and NIST ASD Team (2014). NIST Atomic Spectra Database (version 5.2), [Online], Available: http://physics.nist.gov/asd

[33] J. Nakagawa, R.F. Wormsbecher, D.O. Harris, High-resolution laser excitation spectra of linear triatomic molecules: Analysis of the $B^2\Sigma^+$-$X^2\Sigma^+$ system of SrOH and SrOD, J Mol Spectrosc 97 (1983) 37-64.

[34] J.M. Samaniego, F.N. Egolfopoulos, C.T. Bowman, CO_2* chemiluminescence in premixed flames, Combustion Science and Technology 109 (1995) 183-203.

[35] M. Kopp, M. Brower, O. Mathieu, E. Petersen, F. Guthe, CO_2* chemiluminescence study at low and elevated pressures, Applied Physics B-Lasers and Optics 107 (2012) 529-538.

[36] J.J. Sabatini, E.C. Koch, J.C. Poret, J.D. Moretti, S.M. Harbol, Chlorine-Free Red-Burning Pyrotechnics, Angewandte Chemie-International Edition 54 (2015) 10968-10970.

[37] D. Juknelevicius, L. Mikoliunaite, S. Sakirzanovas, R. Kubilius, A. Ramanavicius, A Spectrophotometric Study of Red Pyrotechnic Flame Properties Using Three Classical Oxidizers: Ammonium Perchlorate, Potassium Perchlorate, Potassium Chlorate, Zeitschrift für anorganische und allgemeine Chemie 640 (2014) 2560-2565.

[38] M.H. Stans, Bond dissociation energies in simple molecules, NIST Special Publication 1 (1970).

[39] R.S. Carter, Molecular dynamics and structure of solids (National Bureau of Standards, 1969).

[40] K.J.R. Rosman, P.D.P. Taylor, Isotopic compositions of the elements 1997, Pure and Applied Chemistry 70 (1998) 217-235.

APPENDICES

Appendix A - PGOPHER Input File (.pgo) for SrO

PGOPHER input files are stored in XML format. To facilitate flexibility and ease of use, a MatLab script was used to generate the XML formatted inputs used by PGOPHER. Below is the content of the resulting PGOPHER input file for the SrO molecular spectrum simulation.

```
<?xml version="1.0"?>
<Mixture Version="Pgopher 9.0.101 04 Jul 2015 11:01 32 bit (fpc 3.1.1 i386-Darwin)"
IntensityUnits="Normalized" PlotUnits="nmAir" ShowParts="True">
  <Species Name="Species" Jmax="200">
    <LinearMolecule Name="SrO" AsymWt="0">
      <LinearManifold Name="X" Initial="False" LimitSearch="True">
        <Linear Name="v=0" S="0" Lambda="Sigma+">
          <Parameter Name="Origin" Value="325.69"/>
          <Parameter Name="B" Value="0.336889"/>
          <Parameter Name="D" Value="3.58793e-07"/>
        </Linear>
        <Linear Name="v=1" S="0" Lambda="Sigma+">
          <Parameter Name="Origin" Value="971.239"/>
          <Parameter Name="B" Value="0.334694"/>
          <Parameter Name="D" Value="3.5431e-07"/>
        </Linear>
        <Linear Name="v=2" S="0" Lambda="Sigma+">
          <Parameter Name="Origin" Value="1608.94"/>
          <Parameter Name="B" Value="0.332459"/>
          <Parameter Name="D" Value="3.49827e-07"/>
        </Linear>
        <Linear Name="v=3" S="0" Lambda="Sigma+">
          <Parameter Name="Origin" Value="2238.74"/>
          <Parameter Name="B" Value="0.330184"/>
          <Parameter Name="D" Value="3.45344e-07"/>
        </Linear>
        <Linear Name="v=4" S="0" Lambda="Sigma+">
          <Parameter Name="Origin" Value="2860.61"/>
          <Parameter Name="B" Value="0.32787"/>
          <Parameter Name="D" Value="3.40861e-07"/>
        </Linear>
        <Linear Name="v=5" S="0" Lambda="Sigma+">
          <Parameter Name="Origin" Value="3474.55"/>
          <Parameter Name="B" Value="0.325517"/>
          <Parameter Name="D" Value="3.36378e-07"/>
        </Linear>
        <Linear Name="v=6" S="0" Lambda="Sigma+">
          <Parameter Name="Origin" Value="4080.59"/>
          <Parameter Name="B" Value="0.323124"/>
          <Parameter Name="D" Value="3.31895e-07"/>
```

```
    </Linear>
    <Linear Name="v=7" S="0" Lambda="Sigma+">
      <Parameter Name="Origin" Value="4678.8"/>
      <Parameter Name="B" Value="0.320691"/>
      <Parameter Name="D" Value="3.27412e-07"/>
    </Linear>
    <Linear Name="v=8" S="0" Lambda="Sigma+">
      <Parameter Name="Origin" Value="5269.28"/>
      <Parameter Name="B" Value="0.318219"/>
      <Parameter Name="D" Value="3.22929e-07"/>
    </Linear>
    <Linear Name="v=9" S="0" Lambda="Sigma+">
      <Parameter Name="Origin" Value="5852.14"/>
      <Parameter Name="B" Value="0.315708"/>
      <Parameter Name="D" Value="3.18446e-07"/>
    </Linear>
    <Linear Name="v=10" S="0" Lambda="Sigma+">
      <Parameter Name="Origin" Value="6427.55"/>
      <Parameter Name="B" Value="0.313157"/>
      <Parameter Name="D" Value="3.13963e-07"/>
    </Linear>
  </LinearManifold>
  <LinearManifold Name="A" Initial="True" LimitSearch="True">
    <Linear Name="v=0" S="0" Lambda="Sigma+">
      <Parameter Name="Origin" Value="11180"/>
      <Parameter Name="B" Value="0.30415"/>
      <Parameter Name="D" Value="0"/>
    </Linear>
    <Linear Name="v=1" S="0" Lambda="Sigma+">
      <Parameter Name="Origin" Value="11797.9"/>
      <Parameter Name="B" Value="0.30303"/>
      <Parameter Name="D" Value="0"/>
    </Linear>
    <Linear Name="v=2" S="0" Lambda="Sigma+">
      <Parameter Name="Origin" Value="12414.6"/>
      <Parameter Name="B" Value="0.30191"/>
      <Parameter Name="D" Value="0"/>
    </Linear>
    <Linear Name="v=3" S="0" Lambda="Sigma+">
      <Parameter Name="Origin" Value="13030.3"/>
      <Parameter Name="B" Value="0.30079"/>
      <Parameter Name="D" Value="0"/>
    </Linear>
    <Linear Name="v=4" S="0" Lambda="Sigma+">
      <Parameter Name="Origin" Value="13645.4"/>
      <Parameter Name="B" Value="0.29967"/>
      <Parameter Name="D" Value="0"/>
    </Linear>
    <Linear Name="v=5" S="0" Lambda="Sigma+">
      <Parameter Name="Origin" Value="14260.2"/>
      <Parameter Name="B" Value="0.29855"/>
```

```
      <Parameter Name="D" Value="0"/>
    </Linear>
    <Linear Name="v=6" S="0" Lambda="Sigma+">
      <Parameter Name="Origin" Value="14874.9"/>
      <Parameter Name="B" Value="0.29743"/>
      <Parameter Name="D" Value="0"/>
    </Linear>
    <Linear Name="v=7" S="0" Lambda="Sigma+">
      <Parameter Name="Origin" Value="15490"/>
      <Parameter Name="B" Value="0.29631"/>
      <Parameter Name="D" Value="0"/>
    </Linear>
    <Linear Name="v=8" S="0" Lambda="Sigma+">
      <Parameter Name="Origin" Value="16105.7"/>
      <Parameter Name="B" Value="0.29519"/>
      <Parameter Name="D" Value="0"/>
    </Linear>
    <Linear Name="v=9" S="0" Lambda="Sigma+">
      <Parameter Name="Origin" Value="16722.4"/>
      <Parameter Name="B" Value="0.29407"/>
      <Parameter Name="D" Value="0"/>
    </Linear>
    <Linear Name="v=10" S="0" Lambda="Sigma+">
      <Parameter Name="Origin" Value="17340.4"/>
      <Parameter Name="B" Value="0.29295"/>
      <Parameter Name="D" Value="0"/>
    </Linear>
  </LinearManifold>
  <TransitionMoments Colour="green" Bra="A" Ket="X">
    <SphericalTransitionMoment Component="auto" Bra="v=1" Ket="v=0"/>
    <SphericalTransitionMoment Component="auto" Bra="v=2" Ket="v=0"/>
    <SphericalTransitionMoment Component="auto" Bra="v=2" Ket="v=1"/>
    <SphericalTransitionMoment Component="auto" Bra="v=3" Ket="v=0"/>
    <SphericalTransitionMoment Component="auto" Bra="v=3" Ket="v=1"/>
    <SphericalTransitionMoment Component="auto" Bra="v=3" Ket="v=2"/>
    <SphericalTransitionMoment Component="auto" Bra="v=4" Ket="v=0"/>
    <SphericalTransitionMoment Component="auto" Bra="v=4" Ket="v=1"/>
    <SphericalTransitionMoment Component="auto" Bra="v=4" Ket="v=2"/>
    <SphericalTransitionMoment Component="auto" Bra="v=4" Ket="v=3"/>
    <SphericalTransitionMoment Component="auto" Bra="v=5" Ket="v=1"/>
    <SphericalTransitionMoment Component="auto" Bra="v=5" Ket="v=2"/>
    <SphericalTransitionMoment Component="auto" Bra="v=5" Ket="v=3"/>
    <SphericalTransitionMoment Component="auto" Bra="v=5" Ket="v=4"/>
    <SphericalTransitionMoment Component="auto" Bra="v=6" Ket="v=2"/>
    <SphericalTransitionMoment Component="auto" Bra="v=6" Ket="v=3"/>
    <SphericalTransitionMoment Component="auto" Bra="v=6" Ket="v=4"/>
    <SphericalTransitionMoment Component="auto" Bra="v=6" Ket="v=5"/>
    <SphericalTransitionMoment Component="auto" Bra="v=7" Ket="v=3"/>
    <SphericalTransitionMoment Component="auto" Bra="v=7" Ket="v=4"/>
    <SphericalTransitionMoment Component="auto" Bra="v=7" Ket="v=5"/>
    <SphericalTransitionMoment Component="auto" Bra="v=7" Ket="v=6"/>
```

```
            <SphericalTransitionMoment Component="auto" Bra="v=8" Ket="v=4"/>
            <SphericalTransitionMoment Component="auto" Bra="v=8" Ket="v=5"/>
            <SphericalTransitionMoment Component="auto" Bra="v=8" Ket="v=6"/>
            <SphericalTransitionMoment Component="auto" Bra="v=8" Ket="v=7"/>
            <SphericalTransitionMoment Component="auto" Bra="v=9" Ket="v=5"/>
            <SphericalTransitionMoment Component="auto" Bra="v=9" Ket="v=6"/>
            <SphericalTransitionMoment Component="auto" Bra="v=9" Ket="v=7"/>
            <SphericalTransitionMoment Component="auto" Bra="v=9" Ket="v=8"/>
            <SphericalTransitionMoment Component="auto" Bra="v=10" Ket="v=6"/>
            <SphericalTransitionMoment Component="auto" Bra="v=10" Ket="v=7"/>
            <SphericalTransitionMoment Component="auto" Bra="v=10" Ket="v=8"/>
            <SphericalTransitionMoment Component="auto" Bra="v=10" Ket="v=9"/>
          </TransitionMoments>
        </LinearMolecule>
    </Species>
    <Parameter Name="Gaussian" Value="0.8"/>
    <Parameter Name="Foffset" Value="0"/>
    <Parameter Name="Temperature" Value="1613"/>
    <Parameter Name="Fmin" Value="740"/>
    <Parameter Name="Fmax" Value="900"/>
</Mixture>
```

Appendix B - PGOPHER Input File (.pgo) for C_2

PGOPHER input files are stored in XML format. To facilitate flexibility and ease of use, a MatLab script was used to generate the XML formatted inputs used by PGOPHER. Below is the content of the resulting PGOPHER input file for the C_2 molecular spectrum simulation.

```
<?xml version="1.0"?>
<Mixture Version="Pgopher 9.0.101 04 Jul 2015 11:01 32 bit (fpc 3.1.1 i386-Darwin)"
IntensityUnits="Arbitrary" PlotUnits="nmAir" ShowParts="True">
<Species Name="C2" Jmax="360">
      <LinearMolecule Name="C2" Symmetric="True" AsymWt="0">
        <LinearManifold Name="a3Pi" Initial="False" LimitSearch="True">
          <Linear Name="v=0" S="2" Lambda="Pi" gerade="False">
            <Parameter Name="Origin" Value="-3.95517e-14"/>
            <Parameter Name="B" Value="1.64062"/>
            <Parameter Name="D" Value="0"/>
          </Linear>
          <Linear Name="v=1" S="2" Lambda="Pi" gerade="False">
            <Parameter Name="Origin" Value="1618.03"/>
            <Parameter Name="B" Value="1.65713"/>
            <Parameter Name="D" Value="0"/>
          </Linear>
          <Linear Name="v=2" S="2" Lambda="Pi" gerade="False">
            <Parameter Name="Origin" Value="3212.73"/>
            <Parameter Name="B" Value="1.67358"/>
            <Parameter Name="D" Value="0"/>
          </Linear>
          <Linear Name="v=3" S="2" Lambda="Pi" gerade="False">
            <Parameter Name="Origin" Value="4784.1"/>
            <Parameter Name="B" Value="1.68997"/>
            <Parameter Name="D" Value="0"/>
          </Linear>
          <Linear Name="v=4" S="2" Lambda="Pi" gerade="False">
            <Parameter Name="Origin" Value="6332.13"/>
            <Parameter Name="B" Value="1.70631"/>
            <Parameter Name="D" Value="0"/>
          </Linear>
          <Linear Name="v=5" S="2" Lambda="Pi" gerade="False">
            <Parameter Name="Origin" Value="7856.83"/>
            <Parameter Name="B" Value="1.72258"/>
            <Parameter Name="D" Value="0"/>
          </Linear>
        </LinearManifold>
        <LinearManifold Name="d3Pi" Initial="True" LimitSearch="True">
          <Linear Name="v=0" S="2" Lambda="Pi" gerade="True">
            <Parameter Name="Origin" Value="19378.5"/>
```

```
            <Parameter Name="B" Value="1.76517"/>
            <Parameter Name="D" Value="0"/>
          </Linear>
          <Linear Name="v=1" S="2" Lambda="Pi" gerade="True">
            <Parameter Name="Origin" Value="21132.1"/>
            <Parameter Name="B" Value="1.78449"/>
            <Parameter Name="D" Value="0"/>
          </Linear>
          <Linear Name="v=2" S="2" Lambda="Pi" gerade="True">
            <Parameter Name="Origin" Value="22848.5"/>
            <Parameter Name="B" Value="1.80353"/>
            <Parameter Name="D" Value="0"/>
          </Linear>
          <Linear Name="v=3" S="2" Lambda="Pi" gerade="True">
            <Parameter Name="Origin" Value="24524.3"/>
            <Parameter Name="B" Value="1.82228"/>
            <Parameter Name="D" Value="0"/>
          </Linear>
          <Linear Name="v=4" S="2" Lambda="Pi" gerade="True">
            <Parameter Name="Origin" Value="26155"/>
            <Parameter Name="B" Value="1.84075"/>
            <Parameter Name="D" Value="0"/>
          </Linear>
          <Linear Name="v=5" S="2" Lambda="Pi" gerade="True">
            <Parameter Name="Origin" Value="27735.2"/>
            <Parameter Name="B" Value="1.85894"/>
            <Parameter Name="D" Value="0"/>
          </Linear>
        </LinearManifold>
        <TransitionMoments Colour="green" Bra="a3Pi" Ket="d3Pi">
          <SphericalTransitionMoment Component="0" Bra="v=0" Ket="v=0"/>
          <SphericalTransitionMoment Component="0" Bra="v=0" Ket="v=1"/>
          <SphericalTransitionMoment Component="0" Bra="v=1" Ket="v=0"/>
          <SphericalTransitionMoment Component="0" Bra="v=1" Ket="v=1"/>
          <SphericalTransitionMoment Component="0" Bra="v=1" Ket="v=2"/>
          <SphericalTransitionMoment Component="0" Bra="v=2" Ket="v=1"/>
          <SphericalTransitionMoment Component="0" Bra="v=2" Ket="v=2"/>
          <SphericalTransitionMoment Component="0" Bra="v=2" Ket="v=3"/>
          <SphericalTransitionMoment Component="0" Bra="v=3" Ket="v=2"/>
          <SphericalTransitionMoment Component="0" Bra="v=3" Ket="v=3"/>
          <SphericalTransitionMoment Component="0" Bra="v=3" Ket="v=4"/>
          <SphericalTransitionMoment Component="0" Bra="v=4" Ket="v=3"/>
          <SphericalTransitionMoment Component="0" Bra="v=4" Ket="v=4"/>
          <SphericalTransitionMoment Component="0" Bra="v=4" Ket="v=5"/>
          <SphericalTransitionMoment Component="0" Bra="v=5" Ket="v=4"/>
          <SphericalTransitionMoment Component="0" Bra="v=5" Ket="v=5"/>
        </TransitionMoments>
      </LinearMolecule>
    </Species>
  <Parameter Name="Gaussian" Value="0.82"/>
  <Parameter Name="Foffset" Value="0"/>
```

```
<Parameter Name="Temperature" Value="1613"/>
<Parameter Name="Fmin" Value="440"/>
<Parameter Name="Fmax" Value="580"/>
</Mixture>
```

Appendix C - CEA Output

This appendix contains the results of the NASA Chemical Equilibrium and Applications (CEA) code for the $SrCl_2$ flame. These results were obtained using an input temperature of 1613-K and pressure of 1-atm.

```
        NASA-GLENN CHEMICAL EQUILIBRIUM PROGRAM CEA2, FEBRUARY 5, 2004
                     BY  BONNIE MCBRIDE AND SANFORD GORDON
       REFS: NASA RP-1311, PART I, 1994 AND NASA RP-1311, PART II, 1996

*******************************************************************************

 prob case=17198462 tp
   p(atm) = 1
   t,k=  1613
 reac
   name H2O(L)          wt%=  3.76
   name CH4             wt%=  8.26
   name Air             wt%= 87.61
   name SrCL2           wt%=  0.37
 output massf
 output trace=1e-10
 end

 OPTIONS: TP=T  HP=F  SP=F  TV=F  UV=F  SV=F  DETN=F  SHOCK=F  REFL=F  INCD=F
 RKT=F  FROZ=F  EQL=F  IONS=F  SIUNIT=T  DEBUGF=F  SHKDBG=F  DETDBG=F
TRNSPT=F

 T,K =  1613.0000

 TRACE= 1.00E-10  S/R= 0.000000E+00  H/R= 0.000000E+00  U/R= 0.000000E+00

 P,BAR =     1.013250

    REACTANT          WT.FRAC   (ENERGY/R),K   TEMP,K  DENSITY
        EXPLODED FORMULA
 N: H2O(L)           0.037600   0.000000E+00     0.00  0.0000
          H  2.00000  O  1.00000
 N: CH4              0.082600   0.000000E+00     0.00  0.0000
          C  1.00000  H  4.00000
 N: Air              0.876100   0.000000E+00     0.00  0.0000
          N  1.56168  O  0.41959  AR 0.00937  C  0.00032
 N: SrCL2            0.003700   0.000000E+00     0.00  0.0000
          SR 1.00000  CL 2.00000
```

SPECIES BEING CONSIDERED IN THIS SYSTEM
(CONDENSED PHASE MAY HAVE NAME LISTED SEVERAL TIMES)
LAST thermo.inp UPDATE: 9/09/04

g 3/98	*Ar	g 7/97	*C	g 8/99	CCL
g 8/99	CCL2	n12/93	CCL3	tpis91	CCL4
tpis79	*CH	g 9/99	CHCL	n12/93	CHCL2
g 7/99	CHCL3	g 4/02	CH2	g12/99	CH2CL
tpis91	CH2CL2	g 4/02	CH3	tpis91	CH3CL
g11/00	CH2OH	g 7/00	CH3O	g 8/99	CH4
g 7/00	CH3OH	srd 01	CH3OOH	g 8/99	*CN
g12/99	CNN	tpis79	*CO	tpis91	COCL
tpis91	COCL2	tpis91	COHCL	g 9/99	*CO2
tpis91	COOH	tpis91	*C2	tpis91	C2CL
g 5/02	C2CL2	tpis91	C2CL3	g 5/02	C2CL4
g 5/02	C2CL6	g 6/01	C2H	g 5/02	C2HCL
g 5/02	C2HCL3	g 1/91	C2H2,acetylene	g 5/01	C2H2,vinylidene
tpis91	C2H2CL2	g 4/02	CH2CO,ketene	g 3/02	O(CH)2O
srd 01	HO(CO)2OH	g 7/01	C2H3,vinyl	g 5/02	C2H3CL
srd 01	CH2CL-COOH	g 9/00	CH3CN	g 6/96	CH3CO,acetyl
g 1/00	C2H4	g 8/88	C2H4O,ethylen-o	g 8/88	CH3CHO,ethanal
g 6/00	CH3COOH	srd 01	OHCH2COOH	g 7/00	C2H5
g 7/00	C2H6	g 8/88	CH3N2CH3	g 8/88	C2H5OH
g 7/00	CH3OCH3	srd 01	CH3O2CH3	g 7/00	CCN
tpis91	CNC	srd 01	OCCN	tpis79	C2N2
g 8/00	C2O	tpis79	*C3	n 4/98	C3H3,1-propynl
n 4/98	C3H3,2-propynl	g 2/00	C3H4,allene	g 1/00	C3H4,propyne
g 5/90	C3H4,cyclo-	g 3/01	C3H5,allyl	g 2/00	C3H6,propylene
g 1/00	C3H6,cyclo-	g 6/01	C3H6O,propylox	g 6/97	C3H6O,acetone
g 1/02	C3H6O,propanal	g 7/01	C3H7,n-propyl	g 9/85	C3H7,i-propyl
g 2/00	C3H8	g 2/00	C3H8O,1propanol	g 2/00	C3H8O,2propanol
srd 01	CNCOCN	g 7/88	C3O2	g tpis	*C4
g 7/01	C4H2,butadiyne	g 8/00	C4H4,1,3-cyclo-	n10/92	C4H6,butadiene
n10/93	C4H6,1butyne	n10/93	C4H6,2butyne	g 8/00	C4H6,cyclo-
n 4/88	C4H8,1-butene	n 4/88	C4H8,cis2-buten	n 4/88	C4H8,tr2-butene
n 4/88	C4H8,isobutene	g 8/00	C4H8,cyclo-	g10/00	(CH3COOH)2
n10/84	C4H9,n-butyl	n10/84	C4H9,i-butyl	g 1/93	C4H9,s-butyl
g 1/93	C4H9,t-butyl	g12/00	C4H10,n-butane	g 8/00	C4H10,isobutane
g 6/01	C4N2	g 8/00	*C5	g 5/90	C5H6,1,3cyclo-
g 1/93	C5H8,cyclo-	n 4/87	C5H10,1-pentene	g 2/01	C5H10,cyclo-
n10/84	C5H11,pentyl	g 1/93	C5H11,t-pentyl	n10/85	C5H12,n-pentane
n10/85	C5H12,i-pentane	n10/85	CH3C(CH3)2CH3	g 2/93	C6H2
g11/00	C6H5,phenyl	g 8/00	C6H5O,phenoxy	g 8/00	C6H6
g 8/00	C6H5OH,phenol	g 1/93	C6H10,cyclo-	n 4/87	C6H12,1-hexene
g 6/90	C6H12,cyclo-	n10/83	C6H13,n-hexyl	g 6/01	C6H14,n-hexane
g 7/01	C7H7,benzyl	g 1/93	C7H8	g12/00	C7H8O,cresol-mx
n 4/87	C7H14,1-heptene	n10/83	C7H15,n-heptyl	n10/85	C7H16,n-heptane
n10/85	C7H16,2-methylh	n 4/89	C8H8,styrene	n10/86	C8H10,ethylbenz
n 4/87	C8H16,1-octene	n10/83	C8H17,n-octyl	n 4/85	C8H18,n-octane

n 4/85	C8H18,isooctane	n10/83	C9H19,n-nonyl	g 3/01	C10H8,naphthale
n10/83	C10H21,n-decyl	g 8/00	C12H9,o-bipheny	g 8/00	C12H10,biphenyl
g 7/97	*CL	g 6/95	CLCN	tpis89	CLO
g 7/93	CLO2	tpis89	CL2	tpis89	CL2O
g 6/97	*H	g 6/01	HCN	g 1/01	HCO
tpis89	HCCN	g 6/01	HCCO	tpis89	HCL
g 6/01	HNC	g 7/00	HNCO	g10/01	HNO
tpis89	HNO2	g 5/99	HNO3	g 1/01	HOCL
g 4/02	HO2	tpis78	*H2	g 5/01	HCHO,formaldehy
g 6/01	HCOOH	g 8/89	H2O	g 6/99	H2O2
g 6/01	(HCOOH)2	g 5/97	*N	g 6/01	NCO
g 4/99	*NH	g 3/01	NH2	tpis89	NH3
tpis89	NH2OH	tpis89	*NO	g 4/99	NOCL
g 4/99	NO2	g 4/99	NO2CL	j12/64	NO3
tpis78	*N2	J12/64	N2O	g 6/01	NCN
g 5/99	N2H2	tpis89	NH2NO2	g 4/99	N2H4
g 4/99	N2O3	tpis89	N2O4	g 4/99	N2O5
tpis89	N3	g 4/99	N3H	g 5/97	*O
g 4/02	*OH	tpis89	*O2	g 8/01	O3
g 1/98	*Sr	tpis96	*SrCL	tpis96	SrCL2
tpis96	SrH	tpis96	*SrO	tpis96	SrOH
tpis96	Sr(OH)2	tpis96	Sr2	g 12/0	THDCPD,endo
g 12/0	THDCPD,exo	g11/99	N2H4(L)	n 4/83	C(gr)
n 4/83	C(gr)	n 4/83	C(gr)	n12/84	CH3OH(L)
n12/84	C2H5OH(L)	n 4/85	C6H14(L),n-hexa	n12/88	C6H5NH2(L)
n10/86	C6H6(L)	g11/99	H2O(cr)	g 8/01	H2O(L)
g 8/01	H2O(L)	j 9/65	NH4CL(II)	j 9/65	NH4CL(III)
j 9/65	NH4CL(III)	srd 93	Sr(a)	srd 93	Sr(a)
srd 93	Sr(b)	srd 93	Sr(L)	tpis96	SrCO3(a)
tpis96	SrCO3(a)	tpis96	SrCO3(b)	tpis96	SrCO3(c)
tpis96	SrCO3(L)	tpis96	SrCL2(a)	tpis96	SrCL2(a)
tpis96	SrCL2(b)	tpis96	SrCL2(L)	tpis96	SrH2(a)
tpis96	SrH2(b)	tpis96	SrH2(L)	tpis96	SrO(cr)
tpis96	SrO(cr)	tpis96	SrO(cr)	tpis96	SrO(L)
tpis96	Sr(OH)2(b)	tpis96	Sr(OH)2(a)	tpis96	Sr(OH)2(L)

O/F = 0.000000

	EFFECTIVE FUEL	EFFECTIVE OXIDANT	MIXTURE
ENTHALPY	h(2)/R	h(1)/R	h0/R
(KG-MOL)(K)/KG	0.00000000E+00	0.00000000E+00	0.00000000E+00
KG-FORM.WT./KG	bi(2)	bi(1)	b0i
*H	0.24769579E-01	0.00000000E+00	0.24769579E-01
*O	0.14778342E-01	0.00000000E+00	0.14778342E-01
*C	0.51584850E-02	0.00000000E+00	0.51584850E-02
*N	0.47235711E-01	0.00000000E+00	0.47235711E-01
*Ar	0.28326061E-03	0.00000000E+00	0.28326061E-03
*Sr	0.23340020E-04	0.00000000E+00	0.23340020E-04

```
 *CL                  0.46680040E-04      0.00000000E+00      0.46680040E-04

 POINT ITN      T            H           O           C           N
                    AR          SR          CL
 ADD  SrO(cr)

              THERMODYNAMIC EQUILIBRIUM PROPERTIES AT ASSIGNED
                          TEMPERATURE AND PRESSURE

             REACTANT                    WT FRACTION      ENERGY      TEMP
                                          (SEE NOTE)     KJ/KG-MOL      K
 NAME        H2O(L)                       0.0376000         0.000      0.000
 NAME        CH4                          0.0826000         0.000      0.000
 NAME        Air                          0.8761000         0.000      0.000
 NAME        SrCL2                        0.0037000         0.000      0.000

 O/F=    0.00000  %FUEL=  0.000000  R,EQ.RATIO= 1.535305  PHI,EQ.RATIO=
0.000000

 THERMODYNAMIC PROPERTIES

 P, BAR            1.0132
 T, K             1613.00
 RHO, KG/CU M    1.8219-1
 H, KJ/KG        -1104.50
 U, KJ/KG        -1660.64
 G, KJ/KG        -17969.2
 S, KJ/(KG)(K)    10.4555

 M, (1/n)          24.115
 MW, MOL WT        24.105
 (dLV/dLP)t      -1.00001
 (dLV/dLT)p        1.0002
 Cp, KJ/(KG)(K)    1.6291
 GAMMAs            1.2686
 SON VEL,M/SEC      839.9

 MASS FRACTIONS

 *Ar             1.1316-2
 CH4             5.044-10
 *CO             9.3095-2
 *CO2            8.0751-2
 COOH            9.392-10
 *CL             1.8079-7
 *H              8.6290-7
 HCN             2.8018-8
 HCO             2.1012-9
 HCL             1.2689-3
```

```
 HNC             5.743-10
 HNCO            2.2008-8
 *H2             9.2716-3
 HCHO,formaldehy 4.8835-9
 HCOOH           1.3550-8
 H2O             1.3993-1
 NH2             4.596-10
 NH3             9.0551-7
 *NO             6.1088-8
 *N2             6.6162-1
 *O              1.442-10
 *OH             1.1647-6
 *O2             2.220-10
 *Sr             3.6499-9
 *SrCL           5.7311-7
 SrCL2           9.4065-4
 *SrO            2.635-10
 SrOH            2.4006-7
 Sr(OH)2         5.5707-5
 SrO(cr)         1.7554-3

  * THERMODYNAMIC PROPERTIES FITTED TO 20000.K

    PRODUCTS WHICH WERE CONSIDERED BUT WHOSE MASS FRACTIONS
    WERE LESS THAN 1.000000E-10 FOR ALL ASSIGNED CONDITIONS

 *C              CCL             CCL2            CCL3            CCL4
 *CH             CHCL            CHCL2           CHCL3           CH2
 CH2CL           CH2CL2          CH3             CH3CL           CH2OH
 CH3O            CH3OH           CH3OOH          *CN             CNN
 COCL            COCL2           COHCL           *C2             C2CL
 C2CL2           C2CL3           C2CL4           C2CL6           C2H
 C2HCL           C2HCL3          C2H2,acetylene  C2H2,vinylidene C2H2CL2
 CH2CO,ketene    O(CH)2O         HO(CO)2OH       C2H3,vinyl      C2H3CL
 CH2CL-COOH      CH3CN           CH3CO,acetyl    C2H4
C2H4O,ethylen-o
 CH3CHO,ethanal  CH3COOH         OHCH2COOH       C2H5            C2H6
 CH3N2CH3        C2H5OH          CH3OCH3         CH3O2CH3        CCN
 CNC             OCCN            C2N2            C2O             *C3
 C3H3,1-propynl  C3H3,2-propynl  C3H4,allene     C3H4,propyne    C3H4,cyclo-
 C3H5,allyl      C3H6,propylene  C3H6,cyclo-     C3H6O,propylox
C3H6O,acetone
 C3H6O,propanal  C3H7,n-propyl   C3H7,i-propyl   C3H8
C3H8O,1propanol
 C3H8O,2propanol CNCOCN          C3O2            *C4
C4H2,butadiyne
 C4H4,1,3-cyclo- C4H6,butadiene  C4H6,1butyne    C4H6,2butyne    C4H6,cyclo-
 C4H8,1-butene   C4H8,cis2-buten C4H8,tr2-butene C4H8,isobutene  C4H8,cyclo-
 (CH3COOH)2      C4H9,n-butyl    C4H9,i-butyl    C4H9,s-butyl    C4H9,t-butyl
```

C4H10,n-butane	C4H10,isobutane	C4N2	*C5	C5H6,1,3cyclo-
C5H8,cyclo-	C5H10,1-pentene	C5H10,cyclo-	C5H11,pentyl	C5H11,t-pentyl
C5H12,n-pentane	C5H12,i-pentane	CH3C(CH3)2CH3	C6H2	C6H5,phenyl
C6H5O,phenoxy	C6H6	C6H5OH,phenol	C6H10,cyclo-	C6H12,1-hexene
C6H12,cyclo-	C6H13,n-hexyl	C6H14,n-hexane	C7H7,benzyl	C7H8
C7H8O,cresol-mx	C7H14,1-heptene	C7H15,n-heptyl	C7H16,n-heptane	C7H16,2-methylh
C8H8,styrene	C8H10,ethylbenz	C8H16,1-octene	C8H17,n-octyl	C8H18,n-octane
C8H18,isooctane	C9H19,n-nonyl	C10H8,naphthale	C10H21,n-decyl	C12H9,o-bipheny
C12H10,biphenyl	CLCN	CLO	CLO2	CL2
CL2O	HCCN	HCCO	HNO	HNO2
HNO3	HOCL	HO2	H2O2	(HCOOH)2
*N	NCO	*NH	NH2OH	NOCL
NO2	NO2CL	NO3	N2O	NCN
N2H2	NH2NO2	N2H4	N2O3	N2O4
N2O5	N3	N3H	O3	SrH
Sr2	THDCPD,endo	THDCPD,exo	N2H4(L)	C(gr)
CH3OH(L)	C2H5OH(L)	C6H14(L),n-hexa	C6H5NH2(L)	C6H6(L)
H2O(cr)	H2O(L)	NH4CL(II)	NH4CL(III)	Sr(a)
Sr(b)	Sr(L)	SrCO3(a)	SrCO3(b)	SrCO3(c)
SrCO3(L)	SrCL2(a)	SrCL2(b)	SrCL2(L)	SrH2(a)
SrH2(b)	SrH2(L)	SrO(L)	Sr(OH)2(b)	Sr(OH)2(a)
Sr(OH)2(L)				

NOTE. WEIGHT FRACTION OF FUEL IN TOTAL FUELS AND OF OXIDANT IN TOTAL OXIDANTS

Appendix D - Temperature Fitting of C_2 Spectra with NMT/BESP

In addition to the spectral simulations implemented with PGOPHER, the Nelder-Mead Temperature (NMT) fitting program [21] was also used to independently determine the flame temperature from the recorded spectra of diatomic carbon. NMT implements the Boltzmann Equilibrium Spectrum Program (BESP) routine to iteratively fit spectra using temperature as a fit parameter.

Results of fitting the C_2 recorded spectra with the NMT program are shown in the figures below. The temperatures computed with NMT for experiments 2 and 8 were 1928-K and 1572-K, respectively. These results agree with measurements taken by the thermocouple to within about 22% for experiment 2 and about 3% for experiment 8.

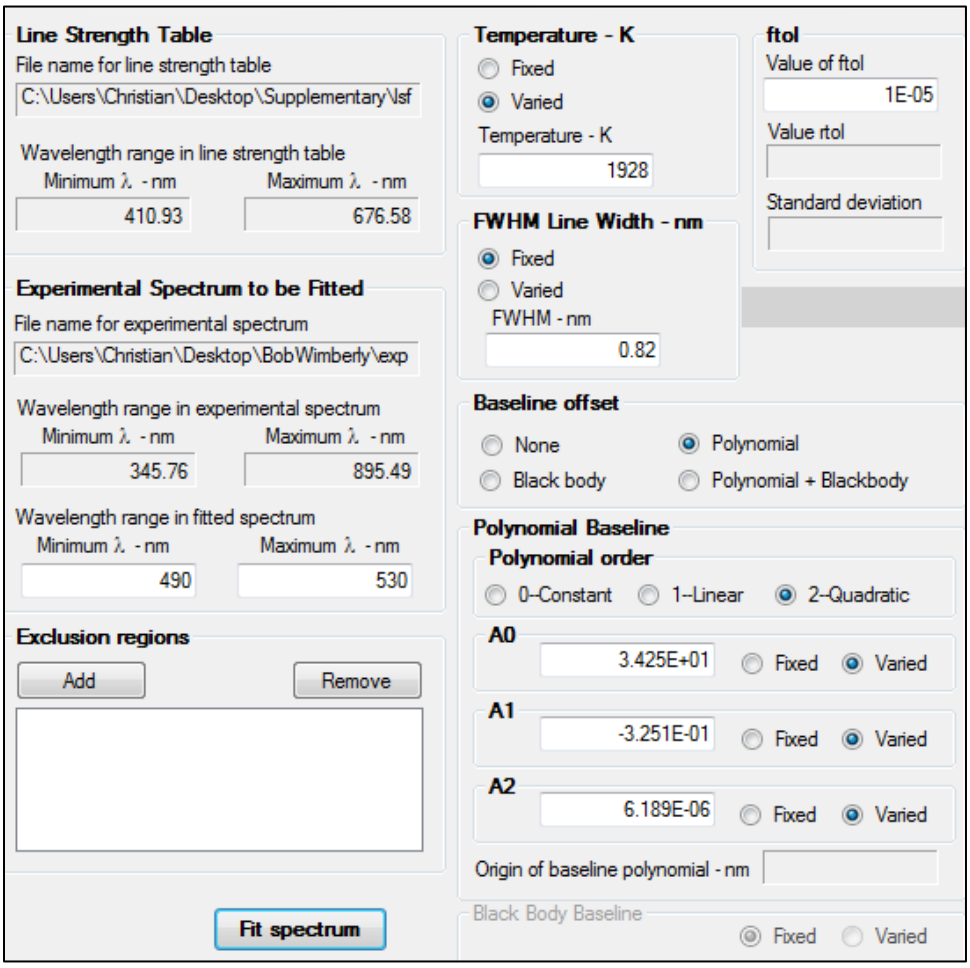


Figure D-1: NMT fit window for experiment 2.

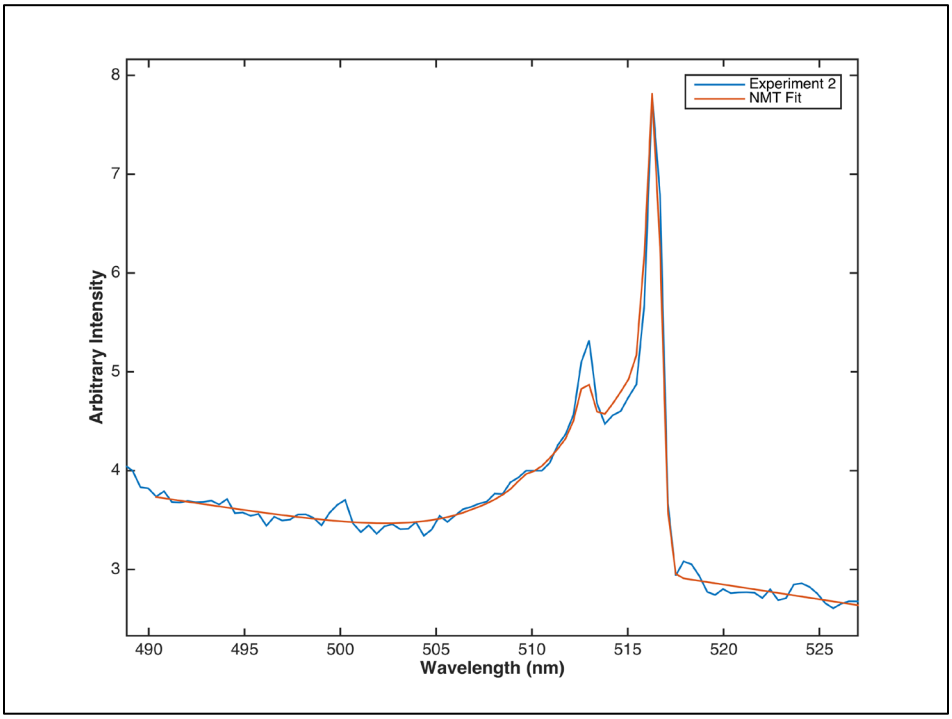


Figure D-2: NMT fitted spectrum versus recorded spectrum for experiment 2.

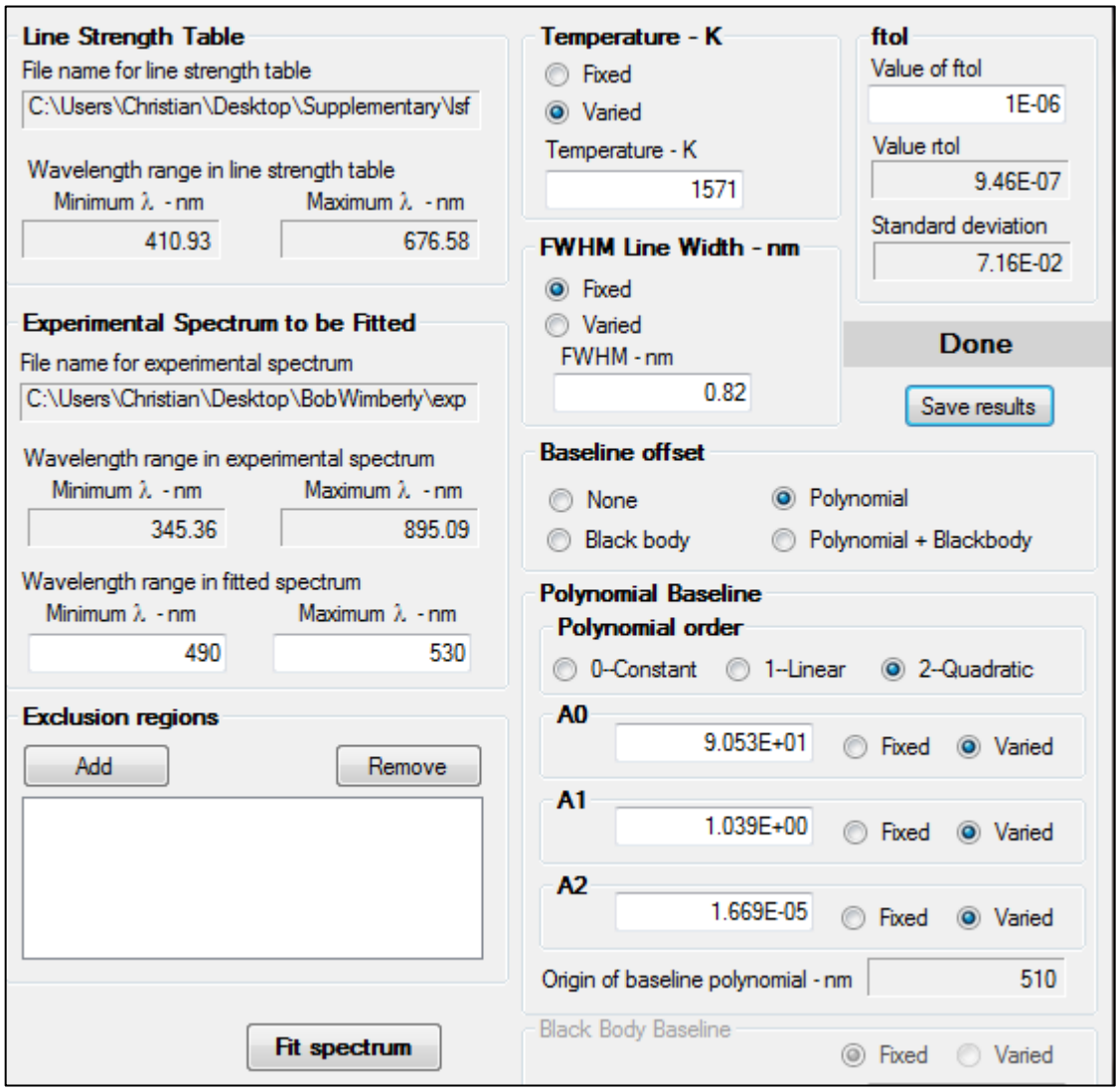


Figure D-3: NMT fit window for experiment 8.

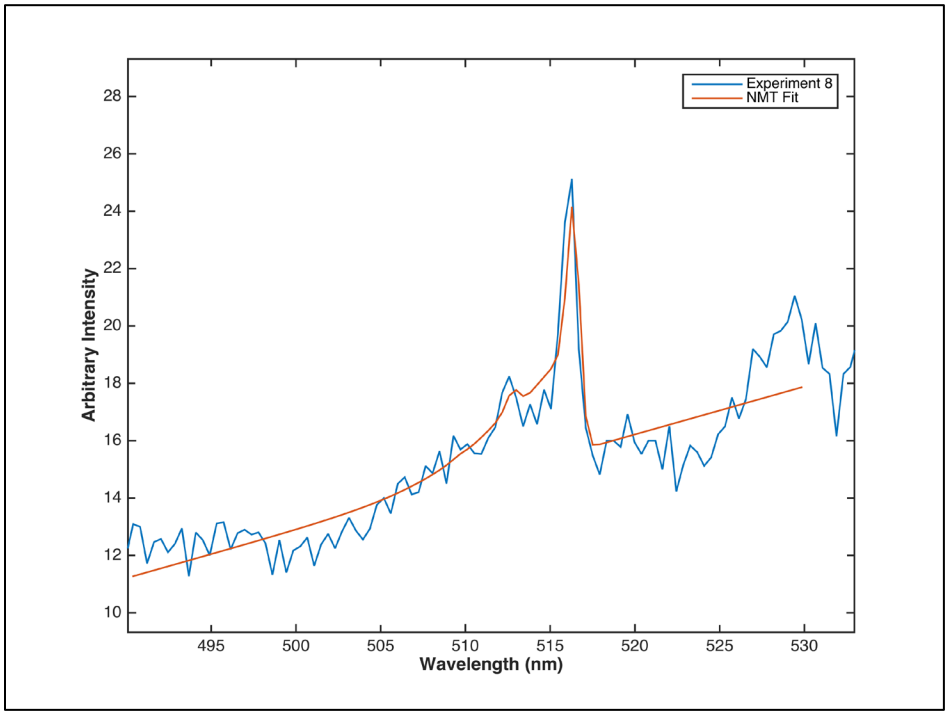


Figure D-4: NMT fitted spectrum versus recorded spectrum for experiment 8.

VITA

Bob Wimberly was born in Blytheville, AR on December 1, 1973. Bob graduated from Lyon County High School in Eddyville, KY in 1992. He pursued his undergraduate degree at Murray State University in Murray, KY where he graduated Magna Cum Laude with a B.S. in Engineering Physics. While there, he was also the recipient of the Outstanding Physics Senior award. After graduation, Bob began working for Sverdrup Technologies at Arnold Air Force Base in 2002. While there, he started pursuing graduate studies at the University of Tennessee Space Institute in Tullahoma, TN where he completed his Master's degree in 2015.